ROOM TEMPERATURE PHOSPHORESCENCE: INVESTIGATION INTO EXTERNAL PERTURBATION OF PVA FILM TO ENHANCE SPIN-ORBIT COUPLING

By

Emma Alexander

Bachelor of Science, 2019
St. Lawrence University
Canton, New York

Master of Science, 2021
Texas Christian University
Fort Worth, Texas

Submitted to the Graduate Faculty of the
College of Science and Engineering
Texas Christian University
in partial fulfillment of the requirements
for the degree of

Doctor of Philosophy

TCU

May 2024

APPROVAL

ROOM TEMPERATURE PHOSPHORESCENCE: INVESTIGATION INTO EXTERNAL PERTURBATION OF PVA FILM TO ENHANCE SPIN-ORBIT COUPLING

by

Emma Alexander

Dissertation **approved:**

Dr. Zygmunt Gryczynski, Major Professor and W.A. "Tex" Moncrief Jr, Chair of Physics

Dr. Hana Dobrovolny, Department Chair and Associate Professor of Physics

Dr. Anton Naumov, Associate Professor of Physics

Dr. Yuri Strzhemechny, Associate Professor of Physics

For the College

ACKNOWLEDGMENTS

I want to thank my advisor, Dr. Zygmunt "Karol" Gryczynski, for allowing me to learn, grow, and become the researcher I am today under his watchful eye. And thank you, Dr. Ignacy Gryczynski for your research support and direction on my PhD journey. They have allowed me to find my path in the world of science and taught me to be creative and assertive and never to lose the enthusiasm to learn. It has been an honor to "pick their brain" and be able to learn from two world renowned researchers.

I am grateful for the advice and support of my committee: Dr. Karol Gryczynski, Dr. Anton Naumov, and Dr. Hana Dobrovolny. I appreciate the effort in considering my work and devoting time to it.

Furthermore, I would like to thank my family. To the Texas Family members, thank you so much for carving out a safe space for me in my journey. And to my New York Family, thank you so much for your undying support and words of encouragement; we had many miles between us, but that never stopped the participation and support of my endeavors.

Among my family members, I want to sincerely thank my Husband, Dalton, who has been my rock through most of my journey. He has sat through many a late night these past five years next to me while I work on my PhD, willing to support me in any way he can.

Finally, I am grateful to my fellow students for their advice and moral support. I am most grateful to the colleagues who have spent time in the lab with me, guiding me, conversing with me, and helping me pursue my Ph.D. To the extent that I would like to extend these special thanks to Dr. Joe Kimball, Dr. Jose Chavez, Dr. Luca Ceresa, Dr. Bong Lee, Michael Seung, Danh Pham, Max Petty, and many other collaborators throughout my years here at TCU.

TABLE OF CONTENTS

LIST OF FIGURES

LIST OF ABBREVIATIONS

$°C$: Celcius

1NH2SO4: Sulfuric Acid

a.u.: arbitrary units

AChE: Acetylcholinesterase

C106: Coumarin 106

CCD: Charge coupled device

CIP: crystallization induced phosphorescence

DAPI: 4′,6-Diamidino-2-phenylindole dihydrochloride

DF: Delayed Fluorescence

DNA: Deoxyribonucleic Acid

E_0: Ground Energy

GmbH: Gesellschaft mit beschränkter Haftung (company with limited liability)

IRF: instrument response function

ISC: Intersystem crossing

K: Kelvin

k_f: radiative decay constant

LED: light emitting diode

M^{-1}: inverse moles

MCP: Microchannel plate

ms: millisecond

MW: molecular weight

n: index of refraction

nm: nanometer

ns: nanosecond

O.D. : optical density

OLED: Organic Light Emitting Diodes

PDL: pulse laser driver

PMT: Photomultiplier tube

PVA: Poly (vinyl) alcohol

QS- Quinine Sulfate

QY- Quantum Yield

RTP: Room Temperature Phosphorescence

s, sec: seconds

S: singlet state

S_0: singlet ground state

S_1: singlet excited state

sec^{-1}: inverse seconds

SOC: Spin Orbit Coupling

T: Triplet state

T_1: Triplet excited state

Trps: Tryptophan

UV: Ultra Violet

cm^{-1}: inverse centimeters

μM: micromole

μs: microsecond

Significance

Currently, there is significant interest in achieving room temperature phosphorescence (RTP) [1], but our knowledge in the field of organic engineering of solid RTP materials remains patchy at best [2]. RTP has many potential applications, including anti-forgery [3-4] and encryption/decryption of information [5]. A wide range of applications for long-lived phosphorescence includes optical sensors (temperature, pH, chemical analytes) [6], bioimaging/diagnostics [2, 7], organic light-emitting diodes [8], photovoltaic equipment, or photodynamic therapy that serves as a very important complementation of oncological treatment [2]. Other less common applications of RTP include printing and visualization of hidden fingerprints in forensic sciences [9].

RTP materials are also used to identify environmental pollution by detecting reactive O_2, typically in quantitative studies measuring the decreasing intensity of phosphorescence [9].

In contrast to fluorescence, which occurs from singlet excited states (S_1 - S_0), phosphorescence is longer in wavelength and occurs at the millisecond to second timescale attributed to the intersystem crossing (ISC) and spin-orbit coupling [10- 12], while also showing unusually high Stokes shift values. However, phosphorescence is generally observed at low temperatures (77 K), and heavy elements are embedded in the fluorophore's chemical structure to induce the spin-orbit coupling.

Moreover, cryogenic conditions have been limited for practical applications of phosphorescence [12- 13], and the use of heavy elements has been restricted due to toxicity-related issues as well as, in some cases, their price, e.g., rare-earth metals, platinum, and iridium [15]. It, therefore, seems

more viable to search for purely organic luminogens, given their better availability and easier applicability [15].

Recent works have focused on the sustainable afterglow room temperature phosphorescence (RTP) from natural resources [16- 17]. The aforementioned phosphorescence capacity of natural products is particularly interesting when one considers that the respective ingredients of such products often contain no conventional chromophores. New phosphorescence phenomena induced by crystallization (CIP) were first discovered in benzophenone crystals and their derivatives at room temperature, whose quantum efficiency can be as high as ~40% [15]. These interesting luminogens show practically no capacity for phosphorescence in solutions or amorphic states but produce very efficient phosphorescence emission in the crystalline form [15].

Crystallization may suppress nonradiative relaxation by limiting interparticle motion. Typically, fluorophores are embedded in solid and/or crosslinked matrix substrates to enhance RTP due to reduced triplet state deactivation (restricted molecular interaction and decreased oxygen diffusion) and enhanced triplet-singlet state transition (interaction of fluorophore with polymer's functional groups) [19]. Adding polymers/biopolymers and crystallization can trigger a similar effect, with the nonradiative relaxation being suppressed by either a rigid medium or a highly efficient network of hydrogen bonds [1, 9, 18].

Merit/Impact

Photonic and electronic properties found in triplet excited states have attracted a great deal of attention for use in next-generation materials and technologies [20- 30]. However, spin flipping is required to efficiently populate the triplet state, which can only be achieved via intersystem crossing (ISC) from the singlet excited state (see Figure 1). This has been facilitated by introducing a heavy atom into the molecular structure. However, for organic molecules without heavy atoms, ISC remains a great challenge, and ISC has extremely low efficiency. Various strategies have been employed to enhance ISC for purely organic molecules, promote spin flipping [24-30], and enhance phosphorescence emission. Notably, the intersystem crossing (ISC) between singlet and triplet states could be promoted by fluctuating the state's energy and the molecule's fluctuation upon self-adaptive resonance [29]. Thus, this effectively forms the basis for the phosphorescence of organic luminophores (Figure 1) [28-30].

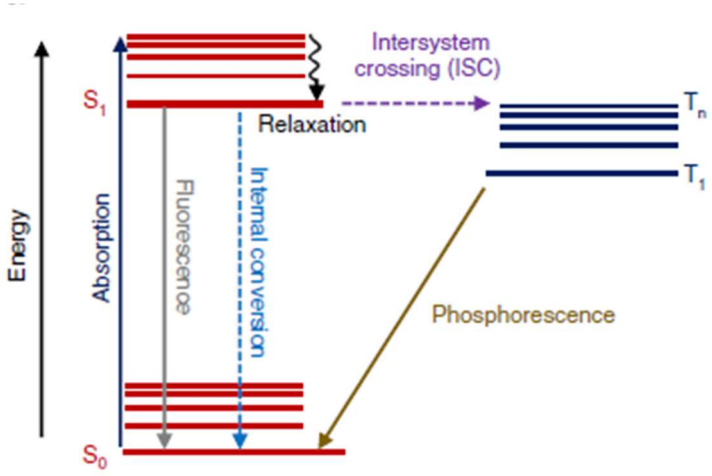

Figure 1. Fundamental mechanism of organic room-temperature phosphorescence (RTP) phenomenon. A: Jablonski diagram illustrating the different photophysical relaxation processes, particularly the intersystem crossing (ISC) between singlet and triplet states, forming the basis for organic luminophores' phosphorescence. [29].

In all studied cases, the triplet excited state has always been populated via singlet state excitation ($S_0 \rightarrow S_1$) and ISC, leading to a triplet excited state ($S_1 \rightarrow T_1$), as shown in Figure 1. The observed phosphorescence is typically weak and is overwhelmed by the fluorescence emission ($S_1 \rightarrow S_0$ transition). Since the emissive lifetime of the triplet state (phosphorescence) is much longer, time-gated detection allows for the separation of the phosphorescence signal from the fluorescence emission, even if phosphorescence is a couple of orders of magnitude weaker. However, the overpowering and overlapping fluorescence emission masked the initial steps of the triplet state evolution/dynamics. The recoverable information may only relate to times longer than the fluorescence lifetime. Consequently, the observed signal is overwhelmed by residual fluorescence and presents low/negative initial anisotropy of phosphorescence. This prevents practical applications of utilizing phosphorescence polarization dynamics.

Creating experimental conditions allowing the triplet state (T_1) to be populated without singlet state excitation would present many advantages for studying triplet state kinetics/dynamics. Multiple earlier approaches (over 60 years ago) that aimed to detect direct triplet state absorption ($S_0 \rightarrow T_1$ transition) in solutions failed, indicating that the cross-section for such absorption is very low, much below measurement error [31- 33]. However, consequent studies by Avakian and Abramon [34] of anthracene crystal and later naphthalene and pyrene crystals presented successful results of singlet-triplet absorption. This shows that highly conjugated crystal packing enhances the probability of spin-forbidden transition.

We recently demonstrated that singlet-triplet direct excitation ($S_0 \rightarrow T_1$ transition) obeys photoselection and produces a high phosphorescence anisotropy [19, 35- 41]. These published reports [19, 35-38] also show that observed phosphorescence is not (minimally) perturbed by indole and indole derivative fluorescence. Notably, due to the lower energy for direct transition,

we could use excitation in the range of 400 nm and above, making it much less harmful than the currently used UV (290 nm) excitation. Technology leading to directly excited RTP would open new and powerful ways for studying protein conformational changes, protein dynamics, protein-protein interactions, and oxygen diffusion/transport in protein systems.

Investigative Questions

Our previous studies concluded that chromophores are perturbed significantly enough to exhibit efficient phosphorescence emission when embedded into the PVA film. Furthermore, we observed that for some compounds embedded into the PVA film, we can observe direct triplet state excitation followed by strong phosphorescence emission. We also noticed that phosphorescence efficiency depends on PVA film preparation. So, we want to investigate modifications in PVA preparation/treatment and how the modifications may enhance Spin-Orbit Coupling (SOC). Our long-term project goal is to investigate if external conditions (conditions we can control/change externally, like electromagnetic fields) can affect SOC and lead to RTP emission in liquid solutions.

1. Characterize the photophysical properties of DAPI in PVA film and C106 in PVA film. Can RTP be distinguishably detected in measurements on these films?
2. Can we directly excite the phosphorescence of the DAPI and C106 films and avoid the traditional ISC route?
3. Using C106 in PVA film, can we alter the phosphorescence with the effects of annealing to produce a greater signal?
4. Looking towards the future of RTP of liquid samples, what can we conclude, if anything, about external perturbations?

Literature Review

Phosphorescence

Phosphorescence has become a major research focus over the recent years with applications in OLED (organic light emitting diodes) [42-45], chemical sensors [46-49], bioimaging [36, 50- 53], and more emerging applications [54-57].

In 1952, Debye and Edwards [58] reported for the first time that phosphorescence could be observed in proteins at cryogenic temperatures. Twenty years later, Saviotti and Galley [59] reported that some proteins in deoxygenated solution present weak room temperature phosphorescence with a long phosphorescence lifetime. Later, Kai and Imakubo [60], Strambini [61-64], Vanderkooi [66-66], Gafni [67,68], and Daganski [69] showed that oxygen quenches the phosphorescence emission of even extraordinarily well-protected Tryptophan (Trps) of alcohol dehydrogenase and alkaline phosphatase with a significant rate constant of 109 M^{-1} sec^{-1} [12]. Thus, when oxygen is present in normal concentrations (250 μM in air-exposed water), phosphorescence emission with an intrinsic lifetime of as long as 5 seconds will be reduced in intensity by a factor of 10^6 and exhibit a lifetime of only a few microseconds. Consequently, RTP has shown great potential, for example, biomedically to study oxygen diffusion in/through proteins, opening the capability to follow protein conformational rearrangements.

When looking at a Jablonski diagram (a simplified one can be seen in Figure 1), there are three ways for the molecule to transition from the excited singlet state back to the ground state after absorption has occurred. One possible transition is a radiative process resulting in fluorescence emission. Fluorescence is the emission of a photon during the process of the molecule returning to its ground state [46]. The second transition is internal conversion, where the transition from the

first excited state is a nonradiative process through multiple vibrational states where energy is lost in the form of heat [70]. Finally, the excited molecule can undergo the process of intersystem crossing (ISC) to the triplet state. From the triplet state, the molecule will then either decay through nonradiative means (internal conversion/ heat) or in a single deactivation step, emitting a photon emission in a process called phosphorescence [46, 70-71]. It's important to remember that the selection rule above is also why the probability of phosphorescence emission, i.e., leaving the triplet state to the singlet ground state, takes 10^4 times longer than the fluorescence emission from an excited singlet state [46].

In principle, the ISC is a nonradiative transition between two electronic states of different multiplicities (singlet to triplet). Crossing between states of different multiplicities is forbidden, but spin-orbit coupling (SOC) can be large enough to make this transition feasible. Due to SOC and depending on the molecule's orbital arrangement, ISC can be more efficient, and phosphorescence rates can prevail over nonradiative rates [71]. Furthermore, studies have shown that an increase in SOC has been shown to increase the radiative rates and decrease the lifetimes of phosphorescence [72]. Due to the processes and interactions mentioned in the above sections, most of the long-lived, bright phosphorescence emission contain heavy metals that help promote SOC [73].

Most organic molecules usually have very low phosphorescence rates at room temperature, so nonradiative pathways dominate [35]. This much weaker phosphorescence is usually dominated by fluorescence or quenched by diffusion or oxygen. To counter this problem, organic molecule phosphorescent studies require careful deoxygenation and low temperatures (77K or lower) [35].

Phosphorescence measurements are typically performed under cryogenic temperatures and inert conditions to limit nonradiative decay pathways exacerbated by temperature, moisture, and oxygen

[74]. Numerous collisions with solvent molecules make phosphorescence in solution at room temperature challenging to detect due to the longer relaxation from the triplet excited state [71]. Heavy atom doping to fluorophores has been used to promote intersystem crossing (ISC) and induce spin-orbit coupling, enabling phosphorescence detection in solution at low temperatures [75-77]. However, these approaches have been restricted by their practical applications under ambient conditions. Transparent and flexible polymer films have often been used to enhance RTP [78]. Non-covalent bonds between the polymer's functional groups and those from fluorophores effectively restrict molecular motion in a solid matrix [79-81]. Oxygen diffusion is decreased, enhancing the fluorophore triplet-singlet state transition [46]. The cost and ease of making polymer films have made it a viable way to detect RTP from novel and existing fluorophores.

DAPI

In the 1970s, DAPI (4′,6-Diamidino-2-phenylindole dihydrochloride) was synthesized and characterized for its remarkable fluorescence properties in the presence of double-stranded DNA [82-84]. DAPI has been widely used to study DNA, as the fluorescence quantum yield of DAPI increased significantly when binding to DNA and various synthetic analogs of different nucleic base sequences [85-88]. The strongest enhancement of DAPI fluorescence has been observed when adjacent to AT-rich regions of DNA [89]. Because of its superior properties, DAPI is now commonly used in microscopy to visualize chromosomes [90-91]. The fluorescence properties of DAPI as a DNA probe have been previously studied using steady-state and time-resolved spectroscopy by Barcelona et al. [92-95]. The structure of electronic transitions of DAPI has been characterized in PVA by linear dichroism and fluorescence excitation anisotropy [96]. DAPI can undergo a photoconversion upon strong UV illumination, resulting in green-to-red emission [97]. Low temperature (77 and 4.2 K) phosphorescence of DAPI and its complexes with

oligonucleotides has also been characterized [98]. The possibility of long-wavelength (over 450nm) excitation of DAPI phosphorescence may have implications that allow for DAPI to extend its use in DNA detection. RTP of DAPI in PVA can be seen in Figure 2.

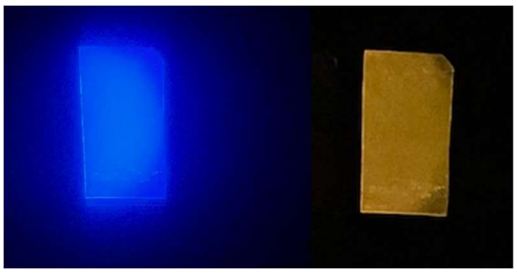

Figure 2. A strip of DAPI in PVA is placed on a UV illuminator. Left: The illuminator is on; right: immediately after the illuminator is off. The green-yellow-gold glow lasts 3-4 s. After a few more seconds, the strip is invisible.

Coumarin 106

A laser dye Coumarin 106 (C106) (also known as Coumarin 478) was synthesized and introduced in the middle of the 1970s [99]. The synthesis aimed to achieve a coumarin derivative with a rigidized, planar molecular structure, which increases fluorescence quantum efficiency in polar solvents. The planar structure of C106 was confirmed by crystallography [100].

Coumarins have recently been used as chemosensors in molecular recognition, molecular imaging, analytical and material chemistry, and biology and medical sciences [101]. In particular, C106 has been found to be an active acetylcholinesterase (AChE) inhibitor [102]. Several smart probes using coumarin have recently been synthesized for metal ion sensing [103].

Room temperature phosphorescence (RTP) of coumarins has been observed on filter papers in the presence of lead acetate as a heavy atom perturber [104]. The C106 in PVA film fluorescence is very strong with a bright blue color; see Figure 3, left. When UV illumination is switched off, the naked eye can see a weaker green glowing phosphorescence for a few moments; Figure 3, right.

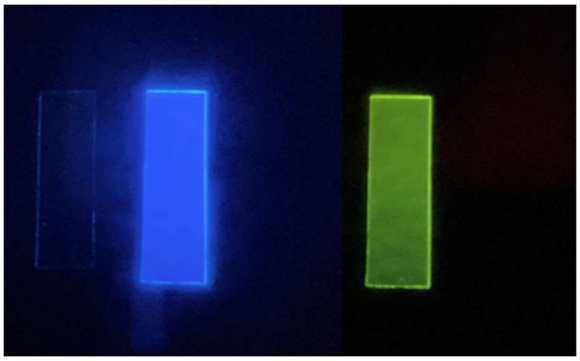

Figure 3. Photographs of PVA strip doped with C106 on a UV illuminator. Left: UV on; Right: UV off. A reference PVA strip is placed on the left side of the C106 strip.

Annealing

Annealing occurs by the diffusion of atoms within a solid material, so the material progresses toward equilibrium. Heat increases the diffusion rate by providing the energy needed to break bonds. The movement of atoms redistributes and eradicates the dislocations in the material. This alteration to existing dislocations allows an object to deform more easily, increasing its ductility [105-107].

Efficient, practical methods of enhancing the properties of the medium and RTP signal are freeze-thaw and annealing [108]. Annealing (thermal treatment) has been applied to PVA doped with silver nanoparticles [109] and carbon films and dots [110-111]. Recently, several reports have appeared on annealing PVA polymers doped with carbon nanodots [112-114]. The impact of the fabrication process on the RTP of small-molecule-doped polymers has been described [115]. All these reports suggest using temperatures below the PVA polymer melting point (about 200°C). In addition to efficient water removal from the PVA film following annealing, structural changes to the polymer structure can appear, changing polymer properties[116-117]. For example, an annealing treatment of 135°C increases the PVA fiber stiffness by 80% [117].

Introduction

Room Temperature Phosphorescence (RTP) of organic and inorganic molecules has been demonstrated as an effective application to encrypt and decrypt information [42] and to prevent counterfeiting [4]. The efficiency of RTP depends highly on the environment. Most molecular systems often use polymer matrices that immobilize organic molecules and shield them from oxygen, i.e., crystals, sol-gels, and doped polymers, to enhance efficiency [43-44]. Poly (vinyl alcohol) (PVA) films are convenient, highly transparent polymers frequently used for luminescence studies. Our lab and others have reported that many organic molecules embedded in PVA films demonstrated exceptionally strong RTP [45,54]. These studies required UV excitation to the S_1 excited state and phosphorescence emission after the intersystem crossing (ISC) transition to the triplet state. Since ISC is a forbidden transition, the observed phosphorescence is weak, and multiple investigations have focused on increasing the emission signal. It has been found that the rigidity of the medium plays an important role in modulating the phosphorescence emission.

Our lab has previously studied indole (and indole derivatives) using a solid polymer substrate to immobilize indole and indole derivatives and observed significant phosphorescence [19, 36-40]. We found that various functional groups or heavy atom substitutions introduced into the indole structures significantly perturb molecular electronic structure and highly enhance spin-orbit coupling between singlet and triplet states. This highly enhances the phosphorescence signal and, in many cases, allows for direct triplet state excitation [19, 38].

Our previous studies concluded that chromophores are perturbed significantly enough to exhibit efficient phosphorescence emission when embedded into the PVA film. Furthermore, we observed that for some compounds embedded into the PVA film, we can observe direct triplet state excitation followed by strong phosphorescence emission. We also noticed that phosphorescence efficiency

depends on PVA film preparation. So, we want to investigate modifications in PVA preparation/treatment and how the modifications may enhance Spin-Orbit Coupling (SOC). Our long-term project goal is to investigate if external conditions (conditions we can control/change externally, like electromagnetic fields) can affect SOC and lead to RTP emission in liquid solutions.

The immediate goal of these studies is to test how polymer preparation and dye-polymer interactions affect SOC. Specifically, we tested different polymer annealing conditions [118], a process known to rigidify polymer matrices. We selected two well-known fluorescence markers, DAPI and Coumarin 106 (C106), for these studies and investigated their fluorescence/phosphorescence properties in the PVA matrix after exposing the PVA to different treatments [41, 119].

Background

Singlet and Triplet States

Let's discuss the case of adding the spin angular momentum of two electrons together. Electrons are fermions with an inherent spin value of $\frac{1}{2}$ [120].

For our example, we will consider that we can measure each electron individually and that subscripts will denote electrons 1 and 2. Therefore, we can write the inherent spin of the electron as

$$s_1 = s_2 = \frac{1}{2} \ , \quad \{Eq.\ 1\}$$

Each electron has a spin vector in which the spin projection is measured in the x, y, and z-direction. These spin vectors are then added together to create the total spin vector of the system.

$$\vec{S} = \vec{S}_1 + \vec{S}_2 \ , \ \{Eq.\ 2\}$$

The eigenvalues can represent the electrons' spin states, $\varepsilon_1, \varepsilon_2$ and their respective eigenvectors, $|\varepsilon_1\rangle, |\varepsilon_2\rangle$. In the case of 2 electrons, there are 4 possible ways the electrons can be added.

$$|\varepsilon_1, \varepsilon_2\rangle = \{|+,+\rangle, |+,-\rangle, |-,+\rangle, |-,-\rangle\} \quad , \{Eq.\ 3\}$$

There exists a basis in which we can describe the sum of the spin of the two electrons as a linear combination of the eigenvectors of our spins.

This basis is the $|S, M\rangle$ basis, where $\vec{S}$ is the is the vector of the total spin and $\vec{M}$ is the vector of the projection of spin onto the S_z axis, and has eigenvalues

$$M = \frac{1}{2}(\varepsilon_1 + \varepsilon_2). \quad \{Eq.\ 4\}$$

Eigenvector M is found to have possible values in the range from $-S$ to $+S$ via whole increments.

$$M = -S, -S + 1, S - 1, S \ , \ \{Eq.\ 5\}$$

Using basis change operations from the $|\varepsilon_1, \varepsilon_2\rangle$ to the $|S, M\rangle$ system, we get 4 possible arrangements. These arrangements all come from possible $\vec{S}$ and $\vec{M}$ combinations.

We can solve the 4 arrangements from here and separate them into singlet and triplet states. When $S = 0, M = 0$, there is only one linear combination of the spin states of the electrons.

$$|0,0\rangle = \frac{1}{\sqrt{2}}(|+,-\rangle - |-,+\rangle) \ , \ \{Eq.\ 6\}$$

This single linear combination possibility is known as the *Singlet State.* The singlet state is non-degenerate, with only one orientation in which the spin of the two electrons can be found, and this orientation is antisymmetric. The ground state of our two electron system is a singlet state.

However, when $S = 1, M = 1,0,-1$, and there are three possible linear combinations of the system

$$|1,0\rangle = \frac{1}{\sqrt{2}}(|+,-\rangle + |-,+\rangle) \ , \ \{Eq.\ 7\}$$

$$|1,1\rangle = |+,+\rangle \ , \ \{Eq.\ 8\}$$

$$|1,-1\rangle = |-,-\rangle \ , \ \{Eq.\ 9\}$$

This is the *Triplet State*. The triplet state is degenerate, meaning there is more than one possible orientation of the two electron spins, and it is symmetric.

It is also clear to see at this point if the singlet state has $S = 0$ and the triplet state has $S = 1$ that, that when a photon moves from singlet to triplet states, the spin angular momentum is not

conserved. The lack of spin angular momentum conservation means that the transition between singlet and triplet state is forbidden.

The example of two measurable electrons is good in theory for two measurables electrons that can be separated individually, but how do we decide the state of electrons when we cannot measure the individual spin? How do we know the ground state is a singlet state?

We can answer the abovementioned questions by looking at the quantum mechanics principles and postulates of identical particles. Identical particles have the same intrinsic properties: mass, spin, charge, etc. Therefore, our system demonstrative system of two electrons is a system of identical particles. Quantum mechanic principles tell us that in a system of two (or more) identical particles, there should be no change in the system's properties or its evolution if the roles of any of the particles are exchanged. This idea of identical particles in classical mechanics is all good. However, in quantum mechanics, the lack of change in the system when the particles switch the order of mention can lead to degeneracies in our results.

The symmetrization postulate is used to solve this degeneracy. From this postulate, we conclude 3 very important ideas for describing identical particles with quantum mechanics.

1. Physical vectors- these vectors explain the physical state space of the particles
2. Depending on the physical vector's nature, they are either symmetric or antisymmetric
3. Bosons are particles with symmetric vectors; fermions are particles with antisymmetric vectors.

To explain mathematically, if we have two identical particles in two states $|\varphi\rangle, |\chi\rangle$ in which these vectors are different, we can express them collectively using a vector of that state.

$$|a\rangle = |1{:}\,\varphi, 2{:}\,\chi\rangle \quad , \{Eq.\ 10\}$$

For bosons, we symmetrize the state, resulting in

$$S|a\rangle = \frac{|1{:}\varphi,2{:}\chi\rangle + |1{:}\varphi,2{:}\chi\rangle}{2} \quad , \quad \{Eq.\ 11\}$$

For fermions, we antisymmetrize the state, resulting in

$$A|a\rangle = \frac{|1{:}\varphi,2{:}\chi\rangle - |1{:}\varphi,2{:}\chi\rangle}{2} \quad , \quad \{Eq.\ 12\}$$

If the two single-particle vectors are identical, find the normalization for bosons is

$$S|a\rangle = \frac{|1{:}\varphi,2{:}\chi\rangle + |1{:}\varphi,2{:}\chi\rangle}{2} = |1{:}\varphi,2{:}\chi\rangle \quad , \quad \{Eq.\ 13\}$$

and fermions

$$A|a\rangle = \frac{|1{:}\varphi,2{:}\chi\rangle - |1{:}\varphi,2{:}\chi\rangle}{2} = 0 \quad , \{Eq.\ 14\}$$

These equations tells us that there is no vector in which the two fermions are in the same individual state. This principle is known as Pauli's Exclusion Principle.

Pauli's Exclusion Principle dictates that in the ground state, the lowest energy state where the two electrons can be found in the same state will not have a matching spin, and thus, the ground state is a singlet state. It also helps to explain the forbidden transition to a triplet state. To go from a singlet state to a triplet state changes the symmetry of the system from the symmetry the molecules naturally orient to, meaning the triplet state is a less probable state to be found naturally without a perturbation to the system [120-123].

Spin-Orbit Coupling

As we discussed previously, singlet and triplet states have different total spins. Due to selection rules, a molecule is allowed to transition between two states so long as the change in spin (ΔS) is equal to zero, $S = 0$ [124]. This selection rule tells us there is a low probability for a molecule to transition from the ground singlet state to the triplet state ($\Delta S \neq 0$) [70].

However, there are interactions between different multiplicity states via Spin-orbit coupling (SOC) [71]. In essence, SOC splits an atomic orbital into different levels with different energies. The energy split is caused by the magnetic fields created by the interaction of spin (S) and the angular momentum L [125]. The interaction of the S and L is expressed by J, total angular momentum [126]. Total angular momentum can be found in the following,

$$J = L + S, L + S - 1, L + S - 2, \dots, |L - S| \quad , \qquad \{Eq.\ 15\}$$

For a molecule, the lowest value of J must be positive or zero [125]. Thus, the singlet state (S) and the triplet state (T) will split further into different states. For example, T will split into three T states, while S will remain one state [126], see Figure 4.

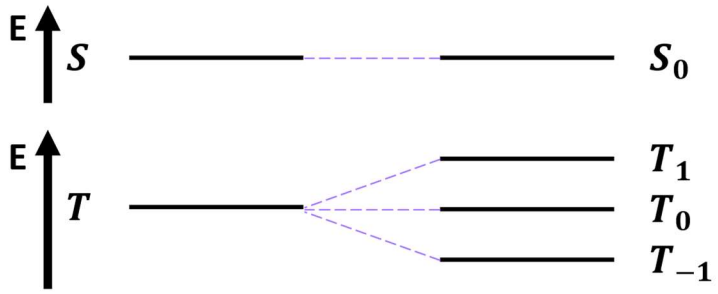

Figure 4. Visual demonstration of how the interaction between S and L (known as J) split the orbital states according to their energies (and angular momentum).

SOC allows for intersystem crossing (ISC), where the molecule goes from an excited singlet state to an excited triplet state before decaying back down and producing a photon [46]. The light produced following ISC is called phosphorescence [46, 70-71].

Theory

Absorbance, Fluorescence and Phosphorescence

The Jablonski diagram, Figure 5, shows a classic energetic representation of molecular energy levels. Each horizontal line represents an energy state, E_i. The bold solid lines represent electronic states, and the thin solid lines represent the vibrational and rotational energy levels. The straight arrows represent pathways involving photons, and the squiggly lines represent nonradiative pathways.

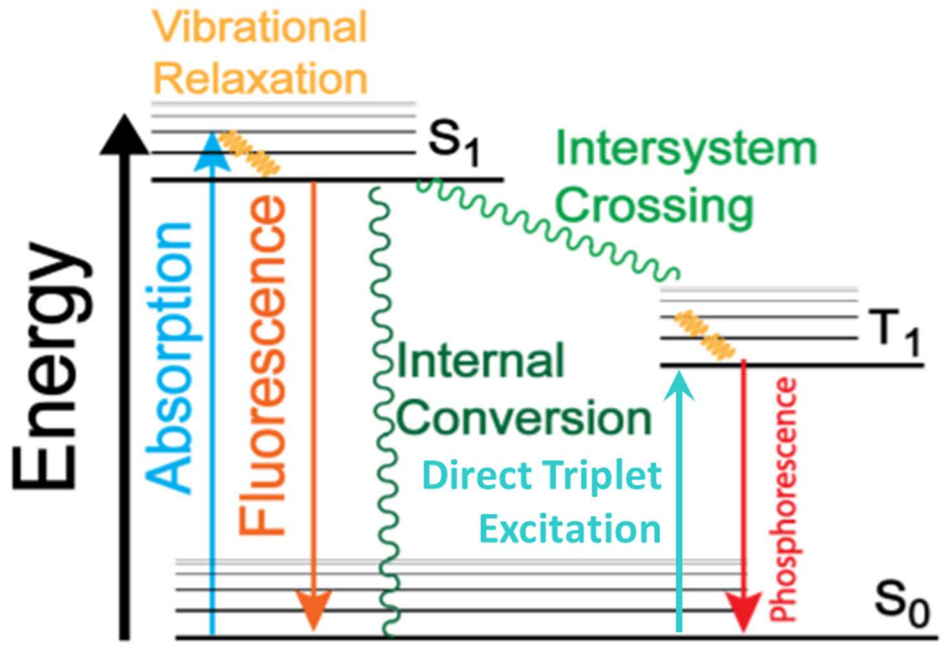

Figure 5. Jablonski Diagram, sometimes referred to as Jablonski-Perrin Diagram [128].

Absorbance

An unperturbed molecule is in the ground state, S_0, with corresponding energy E_0. If the molecule is perturbed by an incoming electromagnetic field, it may transition to an excited state. The

transition into the excited state from the ground state is called the absorption process and happens at a time scale equivalent to 10^{-15}s [129].

Absorption measurements are based on the comparison between the intensity of the incident and the transmitted light. The intensity of light is attenuated as it crosses the sample; the light is transmitted through the cuvette (leaving on the other side), and reaching the detector is indicated as I, see Figure 6.

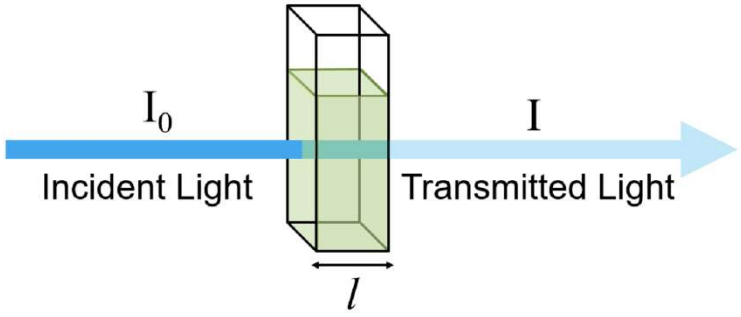

Figure 6. Experimental concept of absorption measurements [130].

The intensity of the transmitted light through the sample is given via the Lambert-Beer Law

$$I = I_0 \cdot e^{-\sigma n l} \text{ , } \{Eq.\ 16\}$$

where n is the number of chromophores per unit volume, l is the path length of the sample that the light travels through (i.e., cuvette width), and σ is the absorption cross-section. The extinction coefficient is typically used instead of the absorption-cross section in photochemistry and photobiology. The extinction coefficient, ϵ, measures how strongly a chemical species or substance absorbs light at a particular wavelength [46]. Converting absorption cross-section to extinction coefficient, we get,

$$\epsilon = \frac{\sigma N_A}{2.303} \text{ , } \{Eq.\ 17\}$$

N_A is Avogadro's Number ($N_A = 6.0225x10^{23} mol^{-1}$). Plugging Equation 17 back into Equation 16, we get a new form of Lambert-Beer Law.

$$I_T = I_0 \cdot 10^{-\epsilon C l} \qquad \{Eq.\ 18\}$$

where C is the concentration of the chromophore and can be calculated from the following conversion

$$C = n * \left(\frac{1000}{N_A}\right) \quad \{Eq.\ 19\}$$

Absorbance (A) is then defined as the argument found in the exponents in the Lambert-Beer Law (Equation 20),

$$A = \epsilon C\ l\ . \quad \{Eq.\ 20\}$$

Excitation Spectra

An excitation spectrum is also run for all of our samples. An excitation spectrum has the emission monochromator set to some wavelength where the sample is known to emit radiation, and the excitation monochromator is scanned through the different wavelengths. An excitation spectrum is usually very similar, if not identical, to an absorption spectrum. An absorbance spectrum measures the wavelengths of light that get blocked/absorbed by the sample, with the peak usually indicating the best wavelength to excite the sample. However, due to the design of the measurement, an excitation spectrum will measure which excitation wavelength causes the most emitted photons of the samples at the wavelength the detector is set. Therefore, any deviation of the excitation spectra from the absorbance spectra may reveal a different activation path, i.e., $S_0 \rightarrow T_1$ [46, 70-71].

Quantum Yield

The quantum yield of a molecule (QY) describes the probability that a photon is emitted when as molecule de-excites to the ground state.

$$QY = \frac{\#\ photo\quad emitted}{\#\ photons\ absorbed} = \frac{\Gamma}{\Gamma + k_{nr}} = \frac{\Gamma}{k} \quad . \quad \{Eq.\ 21\}$$

There are two different forms of molecule deexcitation: radiative emission (photon involved) and nonradiative deactivation (non-photon involved), as seen in Figure 5. We can quantitatively describe the rate at which they occur: radiative (Γ) and nonradiative (k_{nr}), and k is the sum of the radiative and nonradiative rates.

Fluorescence and Phosphorescence

Fluorescence and phosphorescence are possible radiative routes (solid arrows in Figure 5). In these cases, a photon is released, carrying away energy from the molecule. The molecule will then transit to the ground state. Fluorescence is a process that occurs when there is no change in spin multiplicity (S_1 to S_0). The time scale for fluorescence is short, on the order of 10^{-9} seconds (nanoseconds). Phosphorescence occurs when there is a change in the spin multiplicity (T_1 to S_0). This is a spin-forbidden process and, therefore, happens at a relatively slow rate, on the order of 10^{-4} to 10^{2} seconds. There is a third phenomenon called Delayed Fluorescence. Delayed fluorescence is when the molecule sitting in the triplet excited (T_1) state gets a secondary energy source, exciting the molecule back into the singlet excited (S_1) state. This state also has a spin change in its multiplicity, like its phosphorescence counterpart. The time scale of delayed fluorescence is the phosphorescence lifetime (10^{-4} to 10^{2} seconds) plus the fluorescence lifetime (10^{-9} seconds), meaning it will be detected in phosphorescence measurements, not fluorescence measurements [46, 70-71].

Possible nonradiative routes in which energy can be dissipated are collisions $(10^{-10}s)$ with surrounding molecules (heat), internal conversion $(10^{-12}s)$, and dissociation/breaking of bonds from the molecule [46, 70-71, 130].

Stoke's Shift

After absorption, the molecule quickly relaxes $(10^{-13}s)$ into the lowest excited energy state. Fluorescence (or phosphorescence) occurs if a molecule transits back to the ground state and emits a photon. The emitted photon has less energy than the photon that the molecule absorbed due to the nonradiative energy losses, $\left(\Delta E = \frac{hc}{\lambda_{absorbed}} - \frac{hc}{\lambda_{emitted}}\right)$. This change in energy between the absorbed photon and the emitted photon is manifested as Stoke's shift. The emitted photon will have a longer wavelength than the initial absorbed one (i.e., a fluorescein molecule in Figure 7) [46, 70-71, 117, 131].

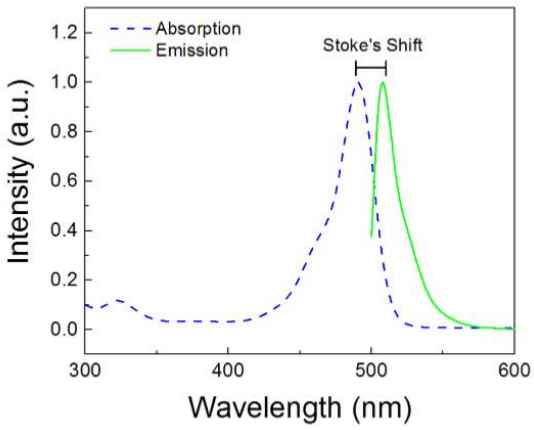

Figure 7. Absorption (dotted blue) and emission (solid green) spectra of 6 μM fluorescein [128].

Time-Resolved Measurements

Fluorescence lifetime is the molecule's average time in the excited state before it transits to the ground state. The definition arises from the fact that the transition of an excited molecule to the ground state is a purely statistical process that can be characterized by a rate constant (probability to transition). The lifetime can then be calculated as the reciprocal of the total decay rates, [46, 70-71].

$$\tau = \frac{1}{\Gamma + k_{nr}} \quad . \quad \{Eq.\ 22\}$$

If the initial number of molecules in the excited state is denoted as N_0, the number of molecules in the excited state as a function of time can be modeled by a first-order rate equation

$$\frac{dN(t)}{dt} = -kN_0(t)\,, \{Eq.\ \ 23\}$$

where k is the total decay rate, $k = \tau + k_{nr}$. Integrating with respect to time gives

$$N(t) = N_0 e^{-kt},\ \ \{Eq.\ \ 24\}$$

Because the definition of a lifetime (Equation 24) is equivalent to $\tau = 1/k$ we get

$$N(t) = N_0 e^{-\frac{t}{\tau}}.\ \ \{Eq.\ \ 25\}$$

Therefore, the average fluorescence lifetime of a single exponential decay is $1/slope$ when the logarithm of the intensity is plotted versus time. Figure 8 is an experimental demonstration of a single decay using $6\mu M$ fluorescein [46, 70-71, 128].

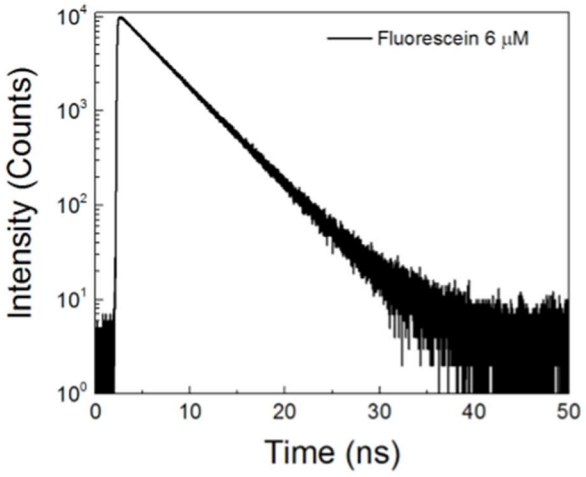

Figure 8. Fluorescence intensity decay of 6 μM fluorescein [128].

A single decay can be modeled using an exponential decay with a time-dependent intensity decay;

$$I(t) = I_0 e^{-\frac{t}{\tau}}\ .\ \ \{Eq.\ \ 26\}$$

Polarization and Anisotropy

When looking in the direction of propagation, polarization can be defined as:

$$P = \frac{I_{\parallel} - I_{\perp}}{I_{\parallel} + I_{\perp}} \ , \quad \{Eq.\ 27\}$$

where $I_{\parallel}$ is the light that is polarized in the same direction as the initial polarization of the incoming light, and $I_{\perp}$ is the intensity of light polarized in the direction perpendicular to the direction of the initial polarization of the incoming light [46, 71, 132].

Equation 27 is effective when all photons observed emitting from the sample travel through the detector. In actuality, photons are emitted from the sample from all directions, not just the direction of the detector. In practice, we only see a fraction of the total photons emitted.

In 1957, Jablonksi derived the general concept of fluorescence anisotropy (r) [133]. Fluorescence anisotropy describes the radiation field rather than just the state of polarization of light through the detector [46, 131-132]. In the case of our work, we use cylindrical symmetry which is described by

$$r = \frac{I_{\parallel} - I_{\perp}}{I_{\parallel} + 2I_{\perp}} \ , \quad \{Eq.\ 28\}$$

where $I_{\parallel}$ is the light that is polarized in the same direction as the initial incoming light and $I_{\perp}$ is the intensity of light polarized in the direction perpendicular to the direction of the initial polarization of the incoming light. With this equation, we now take into account the total light intensity over the entire radiation field.

Anisotropy is commonly defined as in Equation 28. However, anisotropy can also be written in the following form

$$r(\beta) = \frac{2}{5}\left(\frac{3}{2}cos^2\,\beta - \frac{1}{2}\right) = 0.4\left(\frac{3\,cos^2\,\beta - 1}{2}\right) \ , \quad \{Eq.\ 29\}$$

where anisotropy, r, depends only on the angle between the absorption and emission transition moments. There is usually only one emission transition moment because the molecule emits from the lowest excited state. However, there are multiple different absorption transition moments

corresponding to the different energy levels of the molecules. The limits of anisotropy thus are -0.2 and +0.4. The value of 0.4 anisotropy is the maximum value, which is found with isotropic solutions, where $\beta = 0$. -0.2 is the other limit when the transitions between absorption and emission are 90°. The maximum value is often referred to as the "fundamental anisotropy." For all other angles, β, between transition moments, the anisotropy values will range between -0.2 and 0.4 [70-71, 133-138].

Annealing

Annealing is a heat treatment process in which the molecules of a material migrate around the lattice structure without the change in phase state, changing the ductility, hardness [139], or in our case, the phosphorescence [118]. For PVA materials, the temperature for annealing is above the glass transition temperature [140]. The Glass transition temperature is the temperature at which molecular mobility begins; this temperature is dependent of the material in use [141]. In the case of our PVA material, the glass transition temperature is 85 $°C$ [140]. Heating above the glass transition temperatures with PVA will result in stronger interactions between the doped molecule and the polymer chain, which may activate spin-orbit perturbations. This will also explain why some molecules show a stronger phosphorescence enhancement when their shapes fit better to the polymer chain arrangement [118, 140].

Materials and Methods

The Coumarin 106 used is laser grade (purity ≥98%) from Eastman-Kodak. Before use, C106 was recrystallized from a methanol-water solution. The 4′,6-Diamidino-2-phenylindole dihydrochloride (DAPI) used is suitable for fluorescence (purity ≥98%) and is from Millipore Sigma [Sigma Aldrich]. Poly (vinyl alcohol) [MW 130,000, 98% hydrolyzed] was obtained from Millipore Sigma [Sigma Aldrich].

Preparation of the Poly(vinyl alcohol) films

PVA films are prepared from a 10% (w/w) solution of PVA and deionized water. The PVA bulk solution was made in a 500 ml Erlenmeyer flask and was heated/stirred at 95°C until the solution became clear and had a honey-like consistency. The stock solutions of C106 and DAPI were made in 20 ml of 10% (w/w) PVA solution, mixed, and then transferred to an 8.5 cm diameter Petri dish. Blank PVA films were made for background signal corrections. We targeted a film thickness of about 200 microns, accounting for a volume decrease of about 12-13 fold for 10% PVA upon drying [46]. Solutions in Petri dishes were dried at room temperature on a leveled surface. Drying the films in the Petri dishes took about a week; similar preparation is found in [19, 36-40]. After the PVA samples were completely dry, films were pulled from the dishes and cut into strips. The thicknesses of the film strips were measured with a caliper. The film strips were arranged in pairs of sample-reference (PVA filmed doped with C106 and PVA only film) with the same thicknesses. The estimated concentrations of the dyes in PVA films were between 0.5-2.0 mM.

Annealing

Annealing of films was done with a gravity convection lab oven. The temperature was stabilized with ± 2 °C accuracy. The C106 samples were loaded into the preheated oven [118].

Measurements were taken once the samples returned to room temperature. For our experiments we annealed our samples to 150°C, unless otherwise specified. All temperatures used for annealing in our experiments were above the PVA film glass transition temperature of 85 °C [138].

Measurements

Absorption

The Varian Cary 60 UV-Vis Spectrophotometer (Agilent Technologies, Inc.) was used to measure the absorption spectra at room temperature. Each film was measured multiple times, and the absorbances were averaged. Blank PVA was used for baseline corrections unless specified otherwise.The applicability of appropriate average values has been described in [130].

Fluorescence

Fluorescence measurements were conducted on a Varian Cary Eclipse spectrofluorometer (Agilent Technologies, Inc.). Front-face fluorescence measurements were made with a custom-made attachment with a UV grid polarizer on the excitation and a plastic sheet polarizer on the emission [46].

Phosphorescence

Phosphorescence measurements were done in the front-face configuration with a doped PVA strip placed in a 1 mm quartz microcuvette filled with benzene. Benzene is inert to PVA polymer and perfectly matches its refractive index, and because of this, the PVA film appears invisible in benzene, Figure 9. Furthermore, using benzene helps to reduce unwanted reflections.

Figure 9. A PVA strip is placed in an empty 1mm quartz cuvette (left), and after filling the cuvette with benzene (right),

The Varian Cary Eclipse instrument has a mode allowing for time-gated phosphorescence detection. The time-gating mode eliminates the short-lived emission component (Raman scattering, scattering, and fluorescence backgrounds). Unless specified in the figures, the parameters used in this mode were: Total Decay Time: 0.5 s, Number of flashes: 10, Delay Time: 0.3 ms, and Gate Time: 5 ms.

Anisotropy

Excitation and emission anisotropies were calculated from measured polarized intensity components I_{VV} and I_{VH} as

$$r = \frac{I_{VV} - I_{VH} * G}{I_{VV} + 2 I_{VH} * G} \quad . \quad \{Eq.\ 30\}$$

I_{VV} and I_{VH} are phosphorescence intensities measured with a vertically polarized excitation and observed through vertically or horizontally oriented polarizers, respectively. G (G-Factor) has been used to correct the uneven transmissions of I_{VV} and I_{VH} through the detection path. The G-factor was measured for the front-face configuration as described in [55]. Equation 30 has been used for both fluorescence and phosphorescence emission.

Quantum Yield

The fluorescence QY of DAPI in PVA film and C106 in PVA film was estimated by comparing it to quinine sulfate (QS) in 1N H2SO4 fluorescence. The QS solution was placed in a 1 mm thick and 1 cm wide quartz microcuvette. Measurements were done in a front-face configuration in the attachment described in [36].

Time-Resolved Measurements

Fluorescence decay studies were performed using the time-domain method implemented in FluoTime 200 (PicoQuant, GmbH, Germany) equipped with a Hamamatsu microchannel plate detector photomultiplier tube (MCP-PMT). The excitation sources were pulsed laser diodes driven by a PDL-800 driver (PicoQuant, GmbH, Germany). Time-resolved fluorescence data were analyzed using the FluoFit software package (version 4.2.1, PicoQuant, GmbH, Germany). The collected time-dependent intensities were fitted to a single-exponential model as seen in Equation 26.

We used a Varian Cary Eclipse spectrofluorometer (Agilent Technologies, Inc.) for phosphorescence lifetime measurements, equipped with a lifetime function for a sub-second time scale. The gating parameters were the same as the phosphorescence spectra measurements and focused on specific excitation and emission wavelengths, as depicted in the figure captions. The phosphorescence intensity decay was fitted to the single exponential model.

Results and Discussion

DAPI

Absorption, Fluorescence and Phosphorescence

Upon strong UV illumination, DAPI may undergo a photoconversion that produces green-to-red emission [142]. To validate our measurements, we repeated the measurements of each spectrum (absorption, fluorescence, and phosphorescence) a few times. We did not notice any changes in measured intensities, concluding that DAPI molecules are stable in PVA films upon using UV/VIS excitation.

DAPI absorption in PVA film is shifted towards longer wavelengths with a maximum of around 360 nm, see Figure 10.

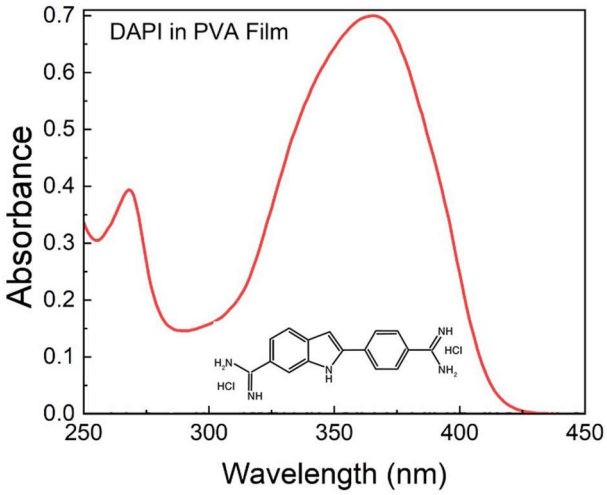

Figure 10. Absorption spectrum of DAPI in PVA film. The peak absorbance is at 360 nm.

However, the fluorescence spectrum is strongly shifted towards shorter wavelengths. The fluorescence maximum in PVA film is about 425 nm (Figure 11).

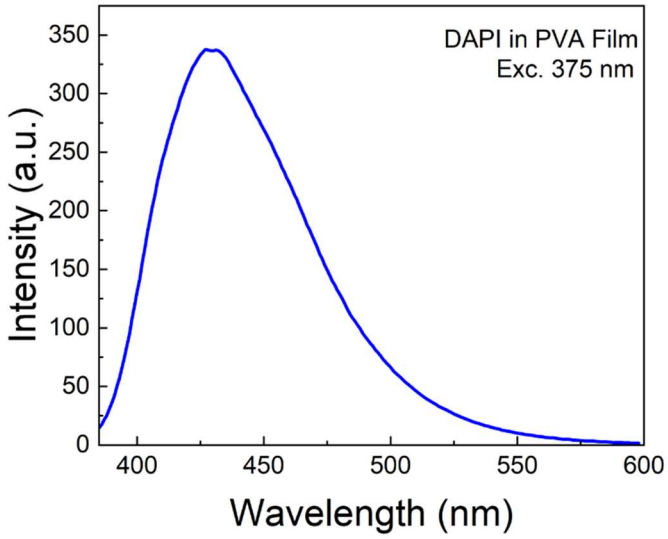

Figure 11. Fluorescence spectrum of DAPI in PVA film. The peak fluorescence when using 375nm excitation is 425 nm.

The fluorescence excitation spectrum of DAPI in PVA film differs from the phosphorescence spectrum at longer wavelengths, see Figure 12. The excitation above 420 nm contains direct triplet state excitation.

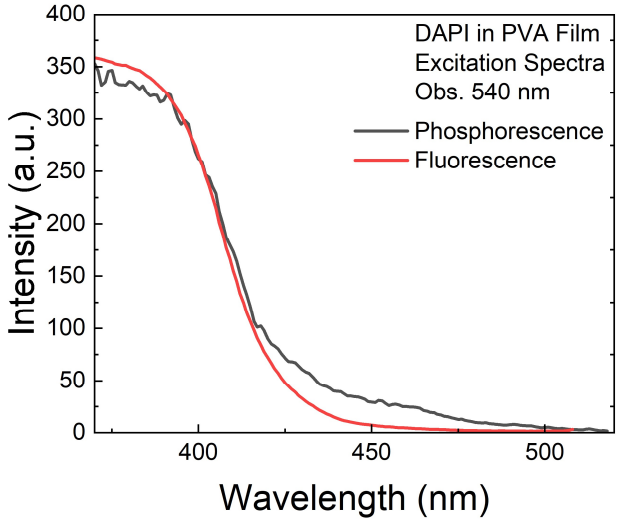

Figure 12. Excitation spectra of phosphorescence (black) and fluorescence (red) of DAPI in PVA film.

The excitation and emission spectra measured with a gated detection are shown in Figure 13.

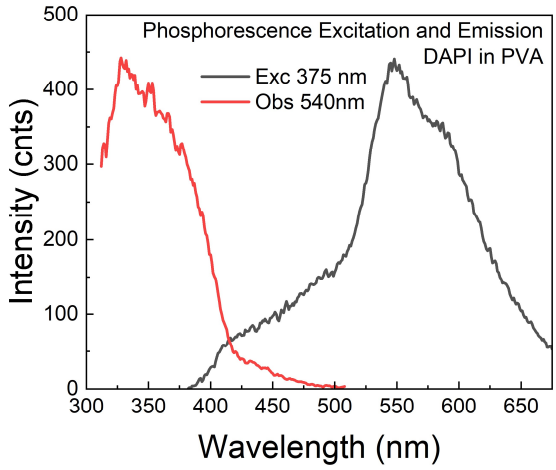

Figure 13. Luminescence spectra of DAPI in PVA film were measured using gated detection. The red line is the excitation spectrum, Black line-emission spectrum. Parameters used for gated detection were total decay-0.5 s, number of flushes- 10, time delay-0.3 ms, and gating-5 ms, which are also described in the Materials and Methods section.

The emission spectrum consists of two bands: delayed fluorescence with a maximum at 425 nm and longer wavelength phosphorescence with a maximum at 550 nm. Figure 14 demonstrates how the gated emission consists of delayed fluorescence and phosphorescence.

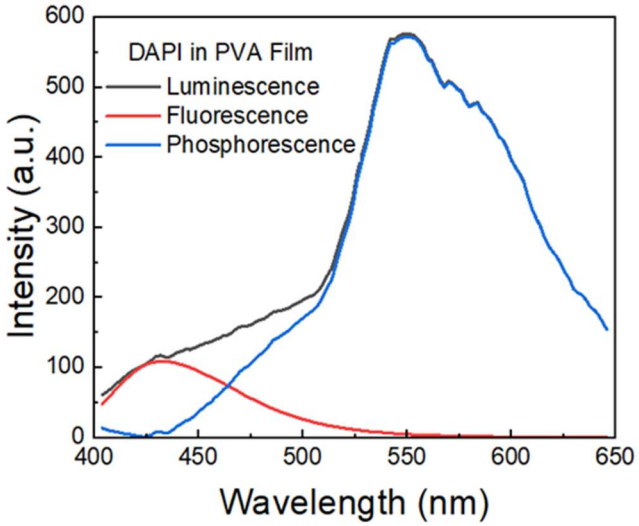

Figure 14. Emission spectra of DAPI in PVA film with gated detection. The total spectrum consists of delayed fluorescence (red) and phosphorescence (blue).

With a commercial instrument (Varian Eclipse), the RTP measurements with the direct triplet state excitation are possible but ineffective, see Figure 15.

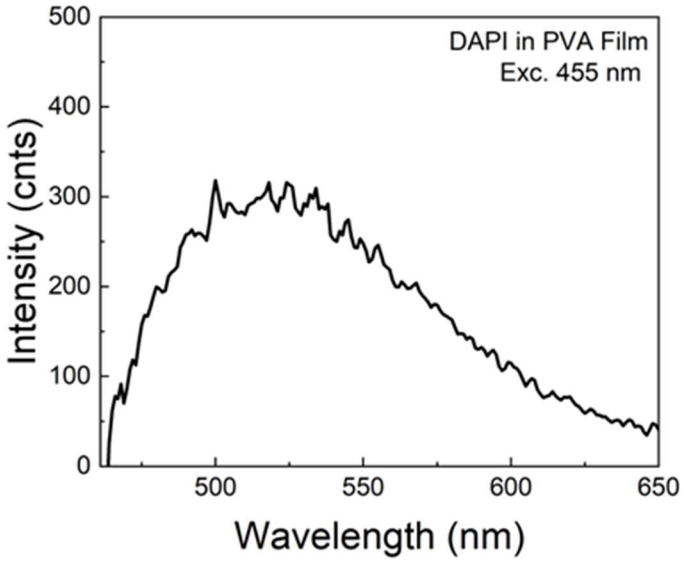

Figure 15. Phosphorescence emission of DAPI in PVA film with a direct triplet state excitation at 455 nm, measured with a commercial spectrofluorometer (Varian Eclipse) using gated parameters described in the Materials and Methods section and in Figure 11 legend.

However, the phosphorescence of DAPI in PVA film can be efficiently excited at longer wavelengths by lasers or LED, see Figure 16. We believe stronger laser excitation and sensitive CCD detectors can be utilized for reliable RTP detection.

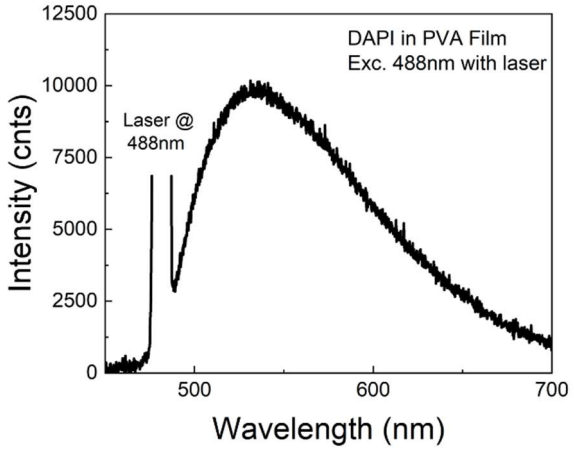

Figure 16. Phosphorescence spectrum of DAPI in PVA film with direct triplet excitation from 488 nm laser. The spectrum was recorded with an Ocean Optics (CCD) spectrometer.

Anisotropy

The estimation of anisotropies requires measurements of vertical and horizontal components of fluorescence emission (excited with a vertically polarized light). Due to the uneven transmission of polarized components through the detection system of the spectrofluorometer, the correction of the horizontal components is necessary, as described in the Materials and Method section.

The fluorescence emission spectrum (Figure 17) and fluorescence excitation spectrum (Figure 18) show high anisotropy values, well above 0.3. This suggests that DAPI molecules are strongly immobilized in the PVA matrix, and depolarizing factors, like energy migration, are negligible.

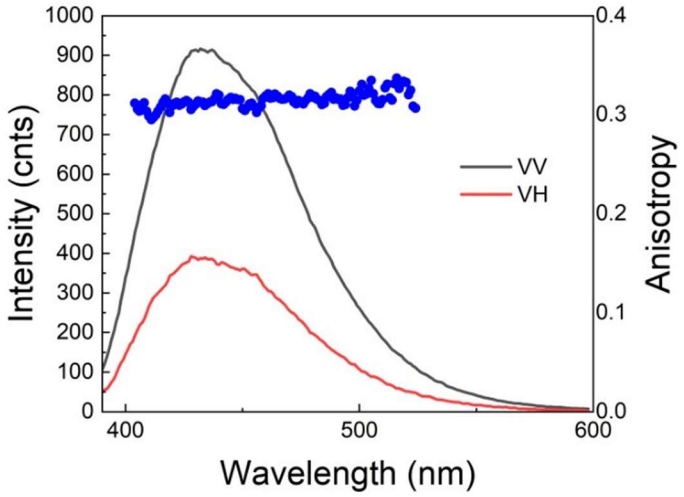

Figure 17. Fluorescence emission anisotropy of DAPI in PVA film. The VV component is in black, and the VH component has been corrected for G-factor and is in red. The anisotropy is high, around 0.3, and shown in blue dots.

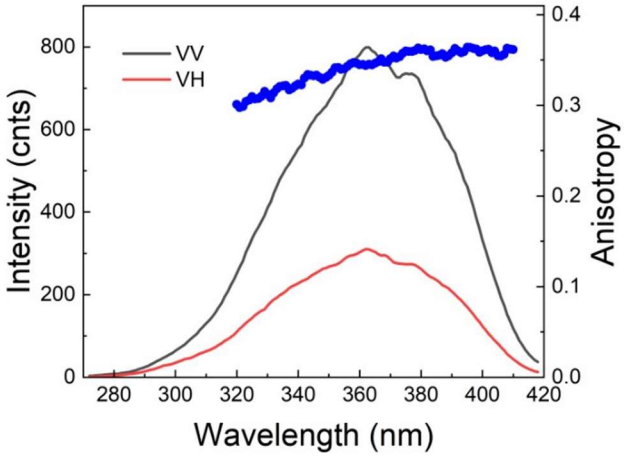

Figure 18. Fluorescence excitation anisotropy of DAPI in PVA film. The VV component is in black, and the VH component has been corrected for G-factor and is in red. The anisotropy is high, around 0.3, and shown in blue dots.

Phosphorescence emission anisotropy is shown in Figure 19. In the phosphorescence band, the anisotropy is negative, about -0.1. This is expected because the transition moment in the triplet state is usually orthogonal to the singlet state, i.e., T_1-S_0 and S_0-S_1 transitions are perpendicular. In the delayed fluorescence band, the anisotropy is positive because, for this emission, the S_1-S_0 transition is responsible.

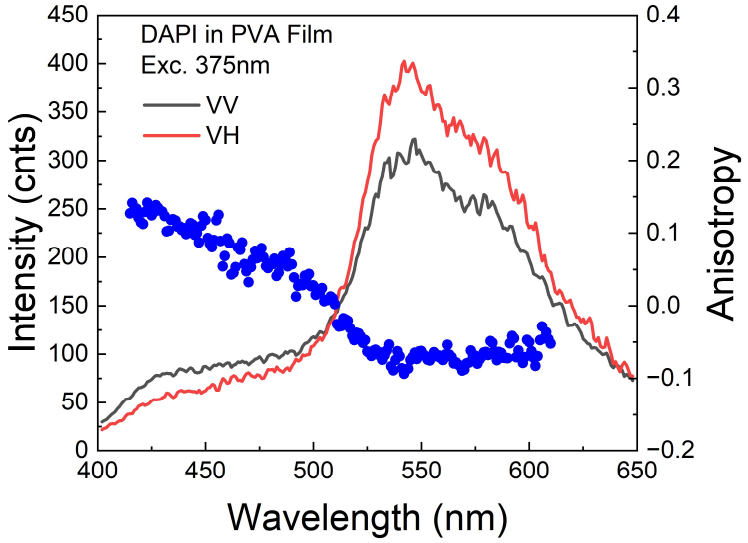

Figure 19. Emission anisotropy of DAPI luminescence in PVA film. The gating parameters are described in the Materials and Methods section and Figure 7 legend. The VV component is in black, and the VH component has been corrected for G-factor and is in red. The anisotropy starts at about 0.1, turns negative around 525 nm, and is shown in blue dots.

The excitation phosphorescence anisotropy, observed in the phosphorescence band, is shown in Figure 20. The excitation to the singlet S_1 state results in negative anisotropy (-0.1). Longer wavelength excitation above 420 nm results in positive and high anisotropy. This is consistent with direct excitation to the triplet state T_1. The absorption and emission transition moments are colinear in such excitation because the intersystem crossing process is not involved.

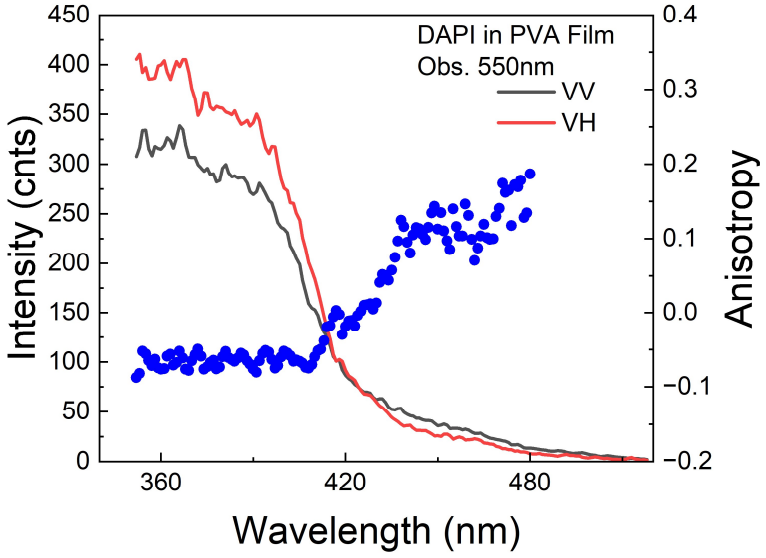

Figure 20. Excitation anisotropy of DAPI luminescence in PVA film. The gating parameters are described in the Materials and Methods section and in the Figure 11 legend. The VV component is in black, and the VH component has been corrected for G-factor and is in red. The anisotropy starts negative (-0.1) around 360nm and turns positive around 420 nm, as shown in the blue dots.

Quantum Yield

We compared fluorescence emission of DAPI in PVA film and Quinine Sulfate in 1NH2SO4 (QS) in 1 mm quartz cuvette. The concentration of QS was adjusted so that its absorbance matched the absorbance of DAPI at 350 nm, see Figure 21.

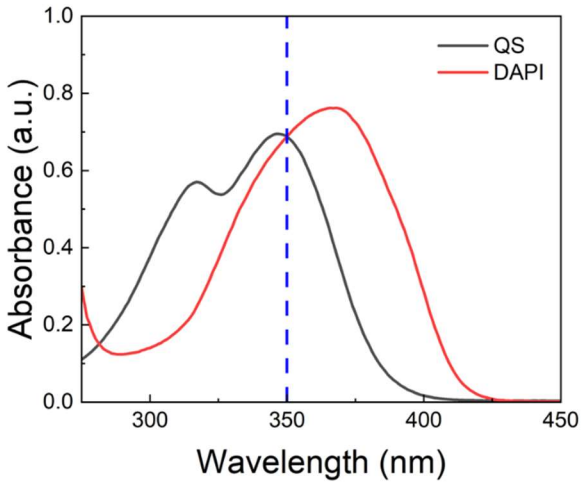

Figure 21. Absorptions of DAPI in PVA film and QS in 1NH2SO4 (1mm quartz micro-cuvette). The blue dotted line marks where DAPI in PVA film and QS in 1NH2SO4 absorbances intersect, 350 nm.

The fluorescence of DAPI in PVA film is very strong, as seen in Figure 22 (the naked eye can see it on the UV illuminator in Figure 6 left).

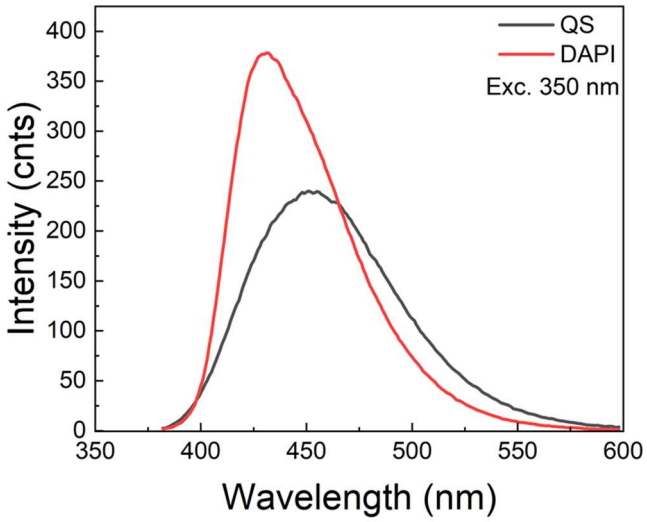

Figure 22. Comparison of fluorescence emission of DAPI and quinine sulfate when excited with 350nm, the wavelength at which the absorbances matched.

Considering the refractive indexes of 1NH2SO4 (n=1.34) and PVA film (n=1.48), the estimated quantum yield of DAPI in PVA film is 0.72.

Knowledge of both the fluorescence and phosphorescence steady-state anisotropies allowed us to reconstruct the phosphorescence spectrum in the red edge of total steady-state emission and estimate phosphorescence quantum yield.

At longer wavelengths above 500 nm, the emission consists of fluorescence and phosphorescence. This is a situation of two emitting species [46]. The observed emission anisotropy is a linear combination of fractional anisotropies: $r = f_F \times r_F + f_P \times r_P$, where symbols F and P refer to fluorescence and phosphorescence, respectively. It should be noted that $f_F + f_P = 1$. Figures 17 and 18 show fluorescence anisotropy is about 0.34 for 375 nm excitation. Phosphorescence anisotropy is about -.08, as seen in Figures 19 and 20, much lower than fluorescence anisotropy. At any long emission wavelength, the measured anisotropy is equal to $(1 - f_P)\, x\, 0.34 + f_P\, x\, (-0.08)$.

We recovered fraction f_P from long-wavelength anisotropy measurements and reconstructed the phosphorescence spectrum, see Figures 23 and 24. The phosphorescence QY of DAPI-doped PVA (estimated by comparing phosphorescence and fluorescence spectral area) is 0.0009. It should be noted this is the ratio of emitted phosphorescence photons to absorbed photons. However, absorption was to the allowed excited singlet state S_1, and phosphorescence occurs from the forbidden triplet state T_1.

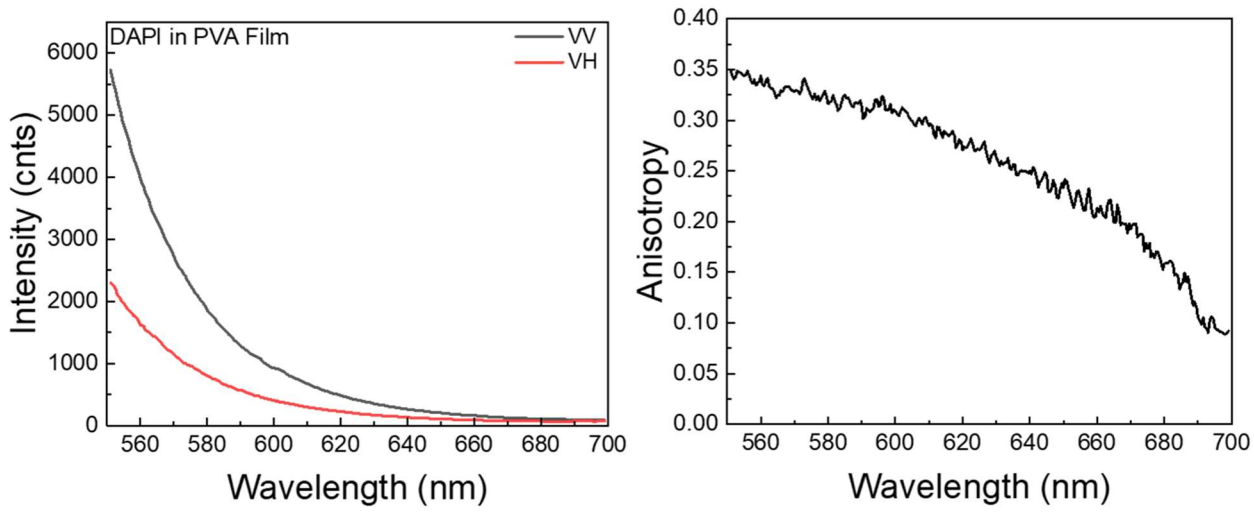

Figure 23. Left: Polarized components of the DAPI-doped PVA film red-edge emission; the VV component is black, and the VH component is red. Right: Steady-state emission anisotropy in the far-red portion of the spectrum. The anisotropy values decrease from 0.35 at 560 to 0.1 around 700 nm.

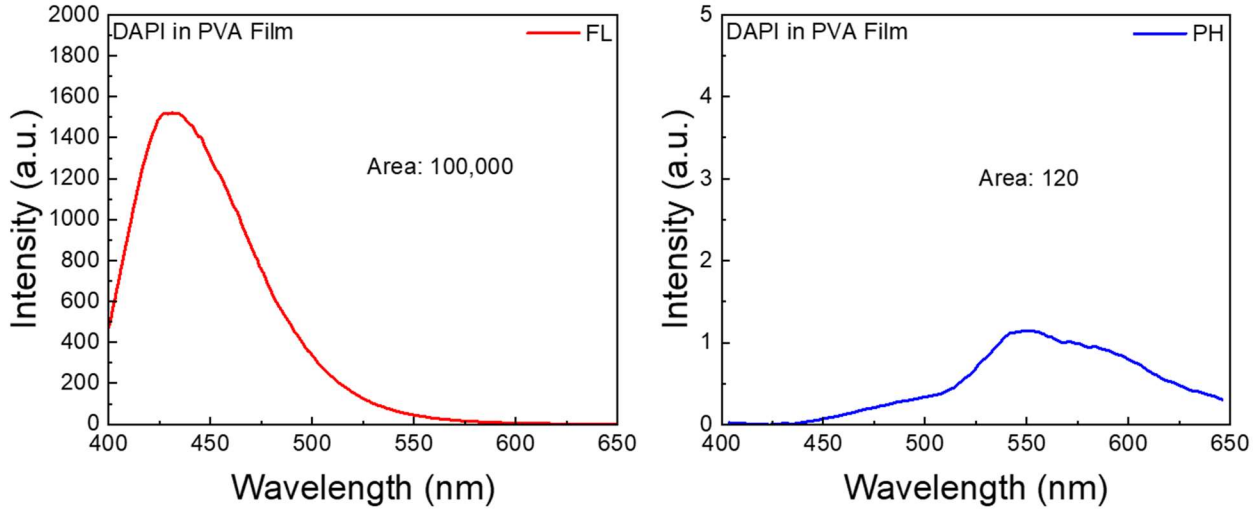

Figure 24. Left: Steady-state emission spectrum of DAPI-doped PVA film. Right: Reconstructed phosphorescence spectrum. Integrated spectra are proportional to the numbers of emitted photons, left: 100,000 emitted photons, right: 120 emitted photons.

Time-Resolved Measurements

The fluorescence intensity decay of DAPI in PVA film is homogeneous, see Figure 25. Considering QY (0.72) and a lifetime of 2.2 ns, the radiative decay constant is $k_f = 0.45$.

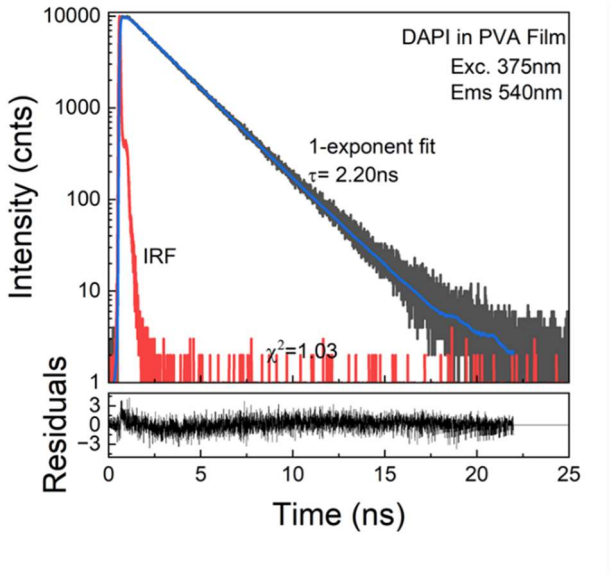

Figure 25. Fluorescence intensity decay of DAPI in PVA film analyzed with single exponent. The measurement was performed with an excitation of 375 nm and observation of 540 nm. IRF is in red, measured intensity decay is black, and the model is in blue. The lifetime, $\tau = 2.20ns$ with a $\chi^2 = 1.03$.

Phosphorescence intensity decay can be satisfactorily approximated with a single exponent model, see Figure 26. The mean lifetime of about 0.3 s is relatively long for RTP.

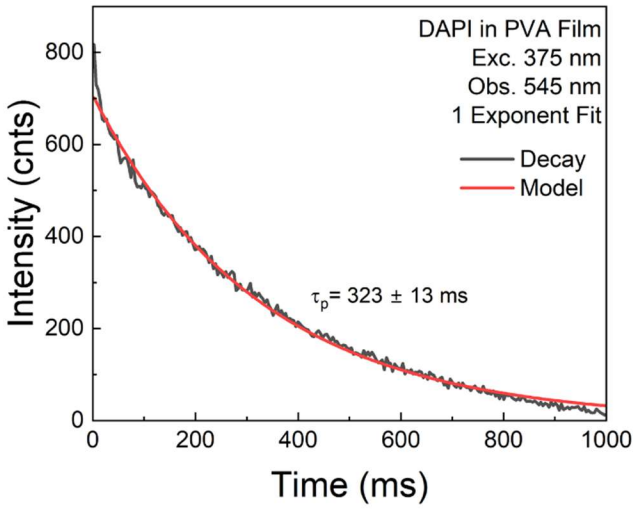

Figure 26. Phosphorescence Emission intensity decay of DAPI luminescence in PVA film analyzed with single exponent. The gating parameters are described in the Materials and Methods section and in Figure 11 legend. The measurement was performed with an excitation of 375 nm and observation of 545 nm. The measured intensity decay is black, and the model is in red. The lifetime, $\tau = 323 \pm 13\ ms$.

Polarity Testing

We checked if DAPI binds to PVA polymer in a liquid phase. The DAPI – PVA solution used for film preparation was compared with a water solution and 85% glycerol, which roughly matched the PVA solution viscosity. Absorption spectra are shown in Figure 27. Compared to DAPI in PVA film, all three absorptions are shifted towards shorter wavelengths. Absorption of DAPI in liquid PVA and DAPI in 85% glycerol are almost identical.

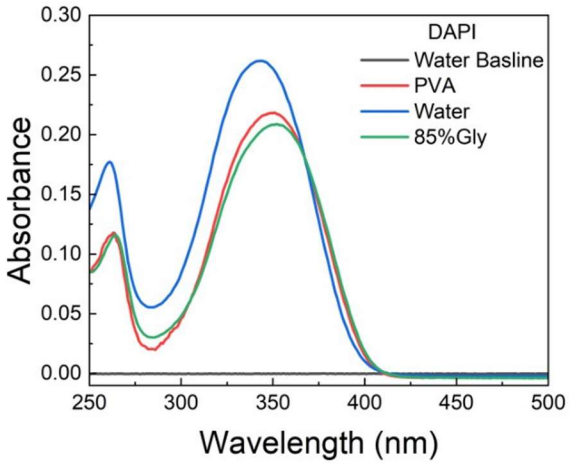

Figure 27. Absorptions of DAPI in liquid PVA (red), in water (blue), and 85% of glycerol (green).

Emission spectra of both DAPI in PVA and 85% glycerol are strongly red-shifted DAPI in water, see Figure 28. Again, the DAPI in liquid PVA and 85% glycerol spectra are similar, except for the intensity. The similarity of absorption and emission spectra with 85% glycerol solution suggests that spectral properties of DAPI in liquid PVA are related to the polarity/viscosity of the solution, not to specific bindings.

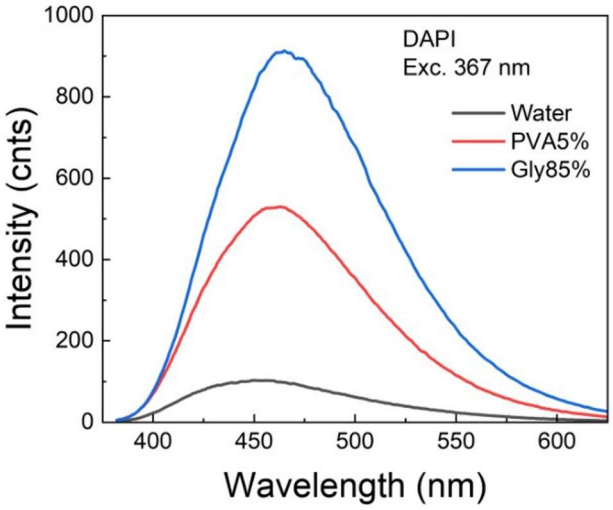

Figure 28. Fluorescence of DAPI in liquid PVA (red), in water (black) and in 85% of glycerol (blue). Both glycerol and PVA are strongly- red shifted to water.

C106 with Annealing Comparison

Absorption, Fluorescence and Phosphorescence

Absorption of C106 in PVA films appears in the UV-Blue spectral region. The long-wavelength band ($S_0 - S_1$) is centered at about 370 nm, see Figure 29.

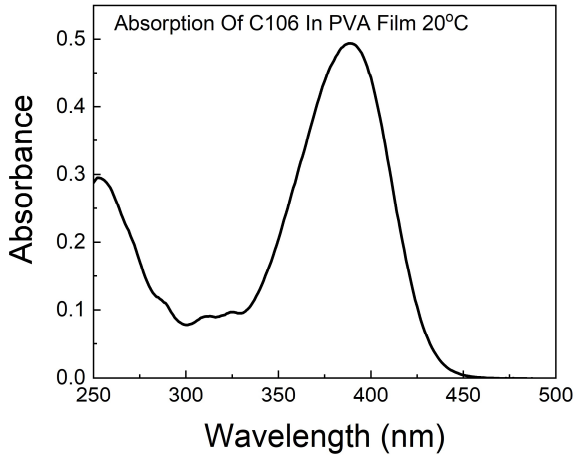

Figure 29. The absorption spectrum of C106 in PVA Film has a peak absorbance at around 370 nm.

A temperature of 150 °C was applied to C106 doped PVA film and to the control sample-PVA film with similar thickness for 15 minutes to anneal the samples.

The absorbances of C106 in PVA films annealed at 150 °C for 15 minutes are compared to non-annealed samples, in Figure 30. The absorbance of the annealed sample increased at shorter wavelengths in UV. This increase is a result of changed PVA absorption.

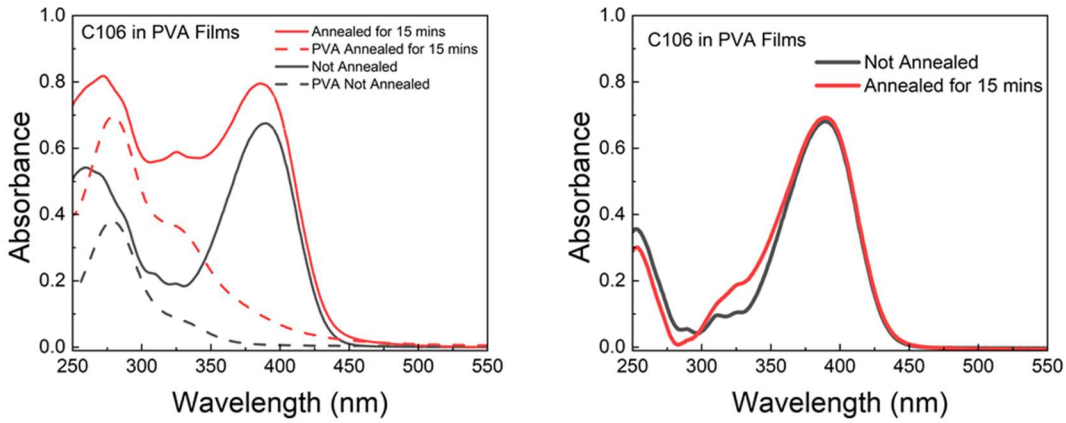

Figure 30. Left: Absorptions of C106 in PVA films for not annealed (black) and annealed at 150^{O}C for 15 min. (red) samples. The absorptions of PVA reference films are shown as dashed lines. These measurements were done with an air as a baseline. Right: Absorptions of C106 in PVA films after subtraction of PVA background. The subtraction shows no change in the absorbance of C106 in PVA at 370nm.

Absorbances of PVA annealed at different temperatures for 15 minutes are shown in Figure 31. Interestingly, annealing at 110 °C practically does not change the PVA absorption. Another series of film strips was annealed at 150 °C for different periods, up to one hour, see Figure 32.

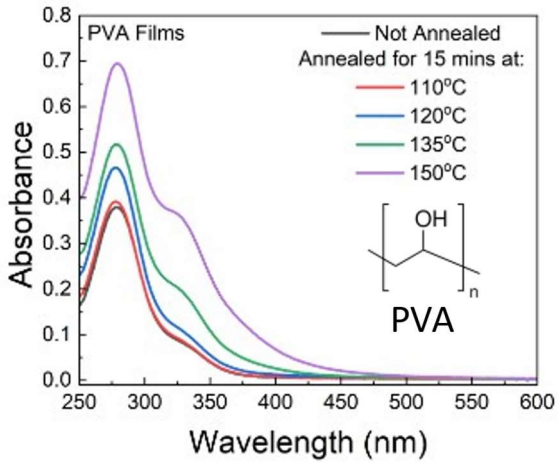

Figure 31. Effect of annealing on the absorption of PVA films. The PVA film strips were heated for 15 minutes at different temperatures. The thicknesses of the films were 0.22 mm.

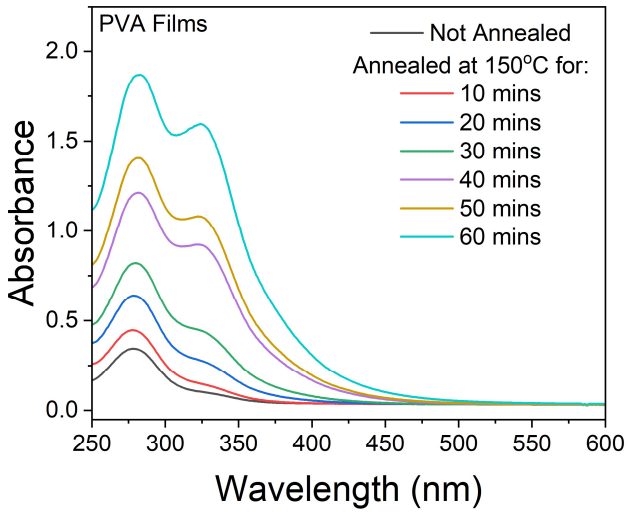

Figure 32. Effect of annealing on PVA films. The strips of PVA films were heated at 150°C for different time periods. The thicknesses of the films were 0.20 mm.

The increase in absorbance seen in Figure 32 was further investigated. Once the not annealed PVA spectra were subtracted from the annealed PVA absorption spectra, we had very similar peaks and increases. The differences between the PVA Annealed films and the not annealed films can be found in Figure 33. We attribute them to the annealing process of the PVA film.

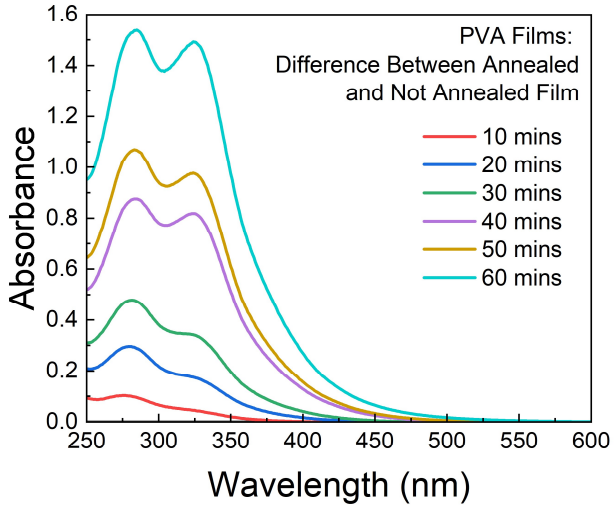

Figure 33. The spectra shown are the difference between the annealed films and the not annealed films at the various times references.

Anyone using UV excitation must consider the PVA absorption for both the absorption of the excitation light and the absorption of fluorescence emission (inner filter effects). Fortunately, the long wavelength absorption of C106 is not strongly overlapped with PVA absorption.

The fluorescence spectrum of C106 with no annealing spans from 400 to 550 nm with a maximum of about 450 nm, see Figure 34.

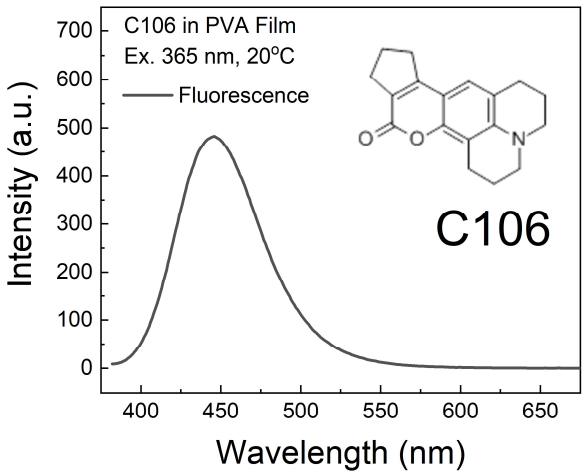

Figure 34. Fluorescence spectrum of C106 in PVA Film. The insert shows a chemical structure of C106. The peak of the fluorescence signal is at about 450 nm.

The fluorescence of C106 in PVA is independent of temperature up to 60°C; see Figure 35. This suggests that either the nonradiative deactivation to the ground state and intersystem crossing to the triplet state do not depend on temperature or both deactivation pathways compensate relatively. If nonradiative deactivation increases, the ISC decreases with temperature. Regardless, the nonradiative deactivation of the excited singlet state is negligible in the case of C106, which confirms its very high quantum yield of fluorescence. Furthermore, we took the logarithmic scale of the intensity to see if there was a shift in the peak wavelength as temperature changed. We found there to be a lack of change at the peaks.

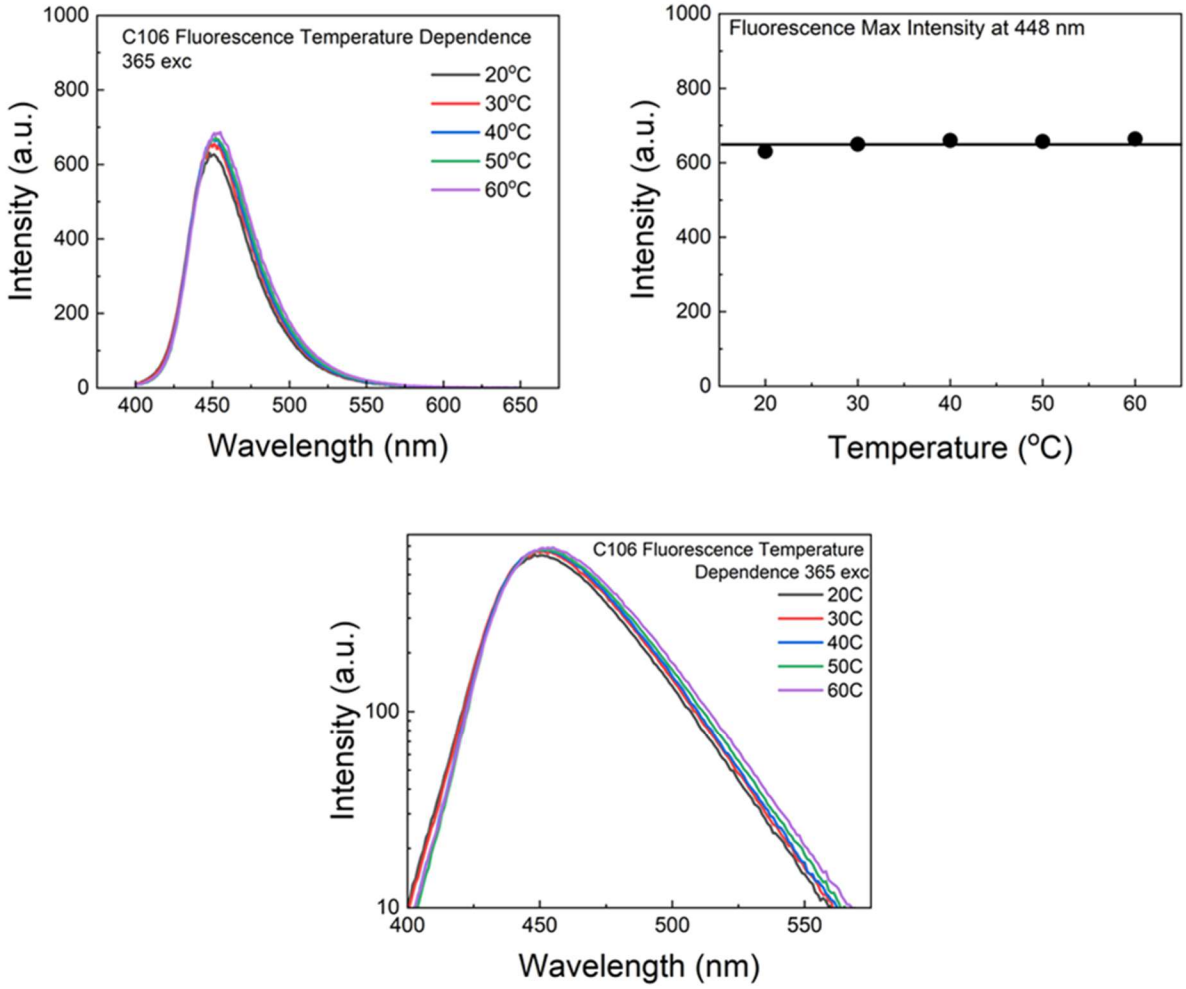

Figure 35. Temperature dependence of C106 in PVA fluorescence. Top Left: spectra. Top Right: fluorescence intensity at 448 nm observation. Bottom: spectra with log scale intensity

We discovered that while the absorption of C106 in PVA films does not depend significantly on annealing, fluorescence emission decreases for annealed samples substantially, see Figure 36. Annealing at 150 °C for 30 minutes results in an almost 50% decrease in fluorescence intensity.

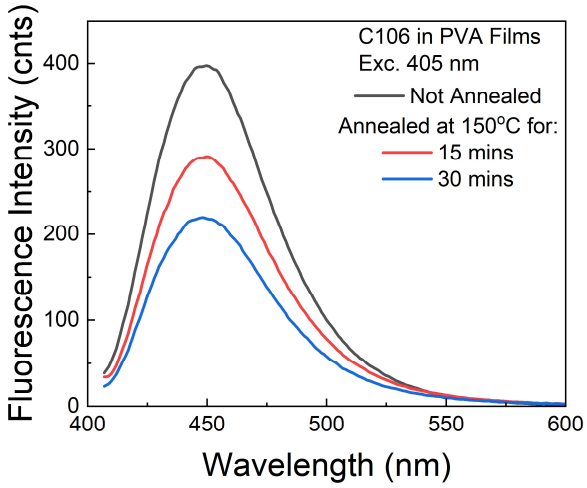

Figure 36. Fluorescence of C106 in PVA film with annealing effects. When annealing at 150 °C at different times: 15 mins (red line) and 30 mins (blue lines), there is a significant decrease in intensity from the not annealed measurement (black lines).

Progressive fluorescence intensity changes at different temperatures are shown in Figure 37. Fluorescence intensity decreases with annealing.

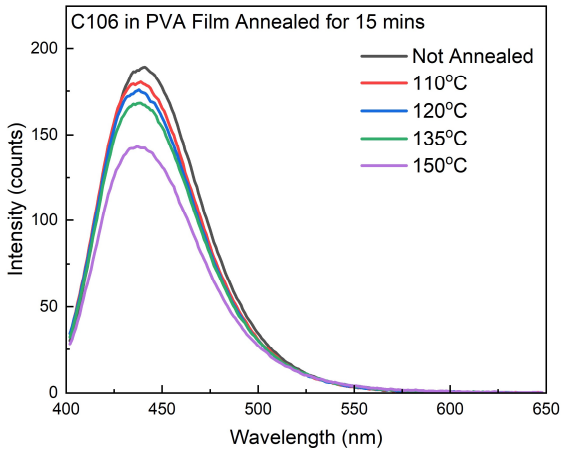

Figure 37. The strips of PVA films doped with C106 were heated for 15 minutes at different temperatures. The not annealed film (black) has the highest intensity, with decreasing fluorescence intensities as the temperature of the film is annealed for 15 minutes. Red line- 110 °C, blue line-120 °C, green line- 110 °C, and purple line 110 °C.

Next, we measured the phosphorescence excitation spectrum of C106 in PVA film, not annealed, see Figure 38.

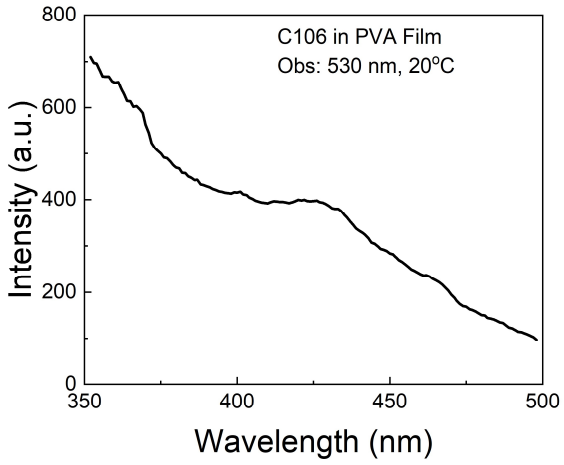

Figure 38. Phosphorescence excitation spectrum of C106 in PVA film. Figure 4, the legend, and the Material and Methods section describe the parameters used for the gated detection.

The long-wavelength part of the phosphorescence excitation spectrum differs significantly from the absorption. We believe the $S_0 - T_1$ absorption is responsible for this difference. Although this transition is forbidden, the interaction of C106 molecules with the polymer matrix results in spin-orbit perturbation, allowing both phosphorescence emission and singlet-to-triplet absorption.

However, with the same sample, we found that the absorption and fluorescence excitation spectra are well matched; see Figure 39.

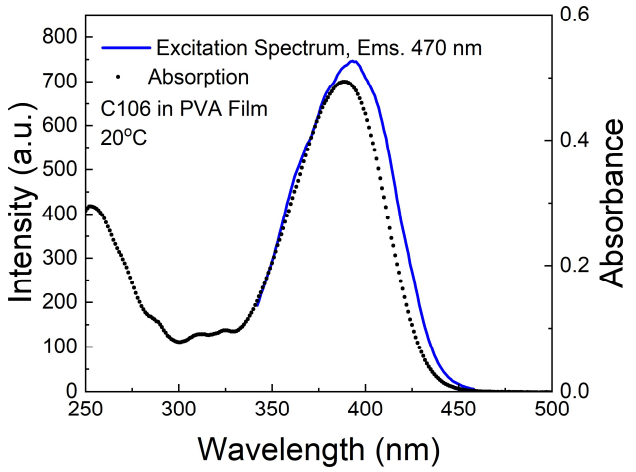

Figure 39. Comparison of C106 absorption and fluorescence excitation spectra. The fluorescence excitation spectra (blue) of C106 in PVA film closely follow the absorbance spectra of C106 in PVA film (black).

This leads us to conclude that the absorption and phosphorescence excitation spectra significantly differ for C106 in PVA, Figure 40. This suggests that the triplet state is not only populated via the singlet excited state. Instead, the triplet state excitation is possible outside absorption (above 450 nm).

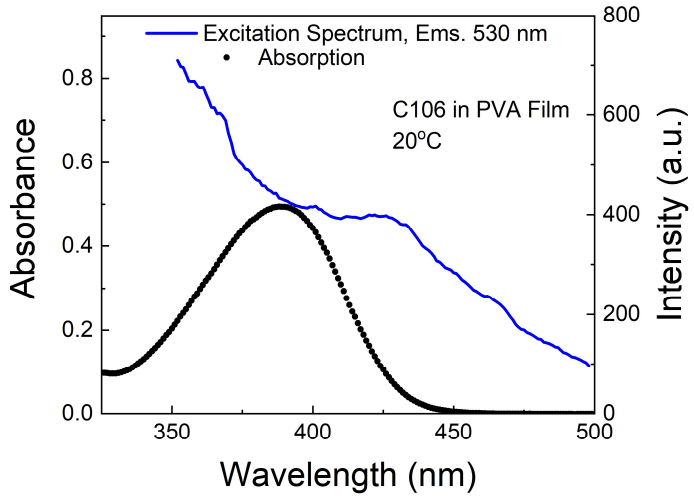

Figure 40. Comparison of C106 absorption and phosphorescence excitation spectra. The phosphorescence excitation spectra (blue) is significantly different than the absorbance spectra (black). This is due to multiple different pathways to excite the triplet state, not just via intersystem crossing.

The phosphorescence excitation spectrum of C106 in PVA film annealed differs from the fluorescence excitation spectrum, see Figure 41. Both spectra measured in fluorescence (blue) and phosphorescence (red) modes were observed at 560 nm with the same slits on excitation and observation paths. Above 450 nm, fluorescence (singlet state) was not excited. At longer wavelengths, the triplet state T_1 of C106 has been directly excited. Furthermore, we calculated the difference between S_1 and T_1 to about 3500 cm^{-1}. The calculation was based on the positions of emission maxima, 450 nm for fluorescence and 535 nm for phosphorescence.

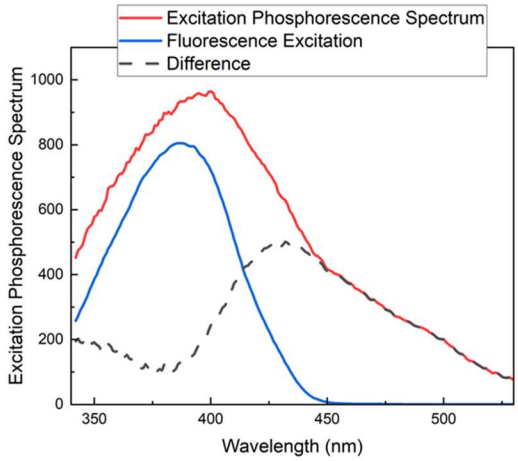

Figure 41. Fluorescence (blue) and phosphorescence (red) excitation spectra of C106 in PVA film annealed for 15 minutes at 150^O C. Subtracting out the fluorescence excitation from the phosphorescence excitation spectra we then get the range in which there is no delayed fluorescence in the phosphorescence excitation (black dashed line).

We found that the C106 in PVA-gated luminescence emission spans from 400 nm to 650 nm; see Figure 42, black. This emission consists of delayed fluorescence (Figure 42, red) and phosphorescence (Figure 42, blue). The wide phosphorescence spectrum is centered at about 530 nm.

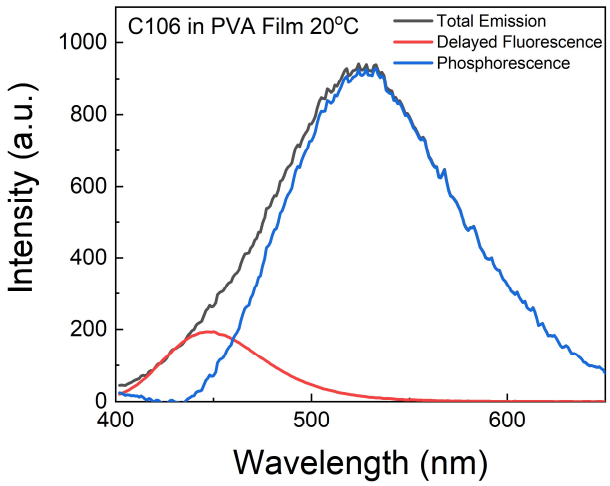

Figure 42. Luminescence spectrum of C106 in PVA film at 365 nm excitation (black). The spectrum consists of delayed fluorescence (red) and phosphorescence (blue). The parameters used for the gated detection were: total decay time- 0.5 s, Number of pulses- 5, delay time- 0.2 ms, and gating- 5 ms.

The phosphorescence emission with long-wavelength excitation at 465 nm (outside the absorbance spectra) results in the spectrum matching precisely the phosphorescence spectrum measured with UV excitation, see Figure 43. Although the phosphorescence with UV excitation is a few times stronger than with long-wavelength excitation, the former offers less unwanted background from the polymer film.

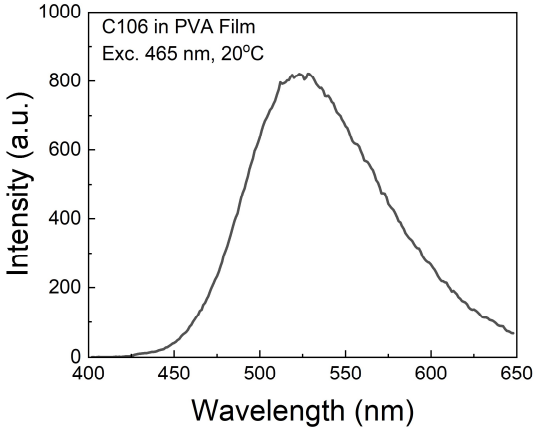

Figure 43. Phosphorescence spectrum of C106 at 465 nm excitation. Parameters used for the gated detection are described in Figure 4 legend and the Material and Methods section. The peak intensity of the phosphorescence spectrum is at 525 nm.

Next, we measured the temperature dependence of phosphorescence emission between 20°C and 60°C for both UV and Blue excitation of C106 in PVA film not annealed.

Up to 60°C, the PVA film remains fairly rigid. First, UV excitation at 365 nm strongly depends on temperature, see Figure 44. However, the short wavelength part of the spectrum, about 450 nm, depends less on temperature. Delayed fluorescence dominates in this wavelength region (see Figure 42). The contribution of delayed fluorescence in the total gated emission is much higher at higher temperatures. The right part of Figure 44 shows the temperature dependence of the maximum gated emission. The emission intensity at 525 nm decreases significantly with temperature.

Furthermore, we took the logarithmic scale of the intensity to see if there was a shift in the peak wavelength as temperature changed. As temperature increases, a bump at 450 nm starts to show. We believe this to be due to delayed fluorescence at this wavelength. The delayed fluorescence, much like regular fluorescence, would not react to environmental temperature changes when these studies are being conducted.

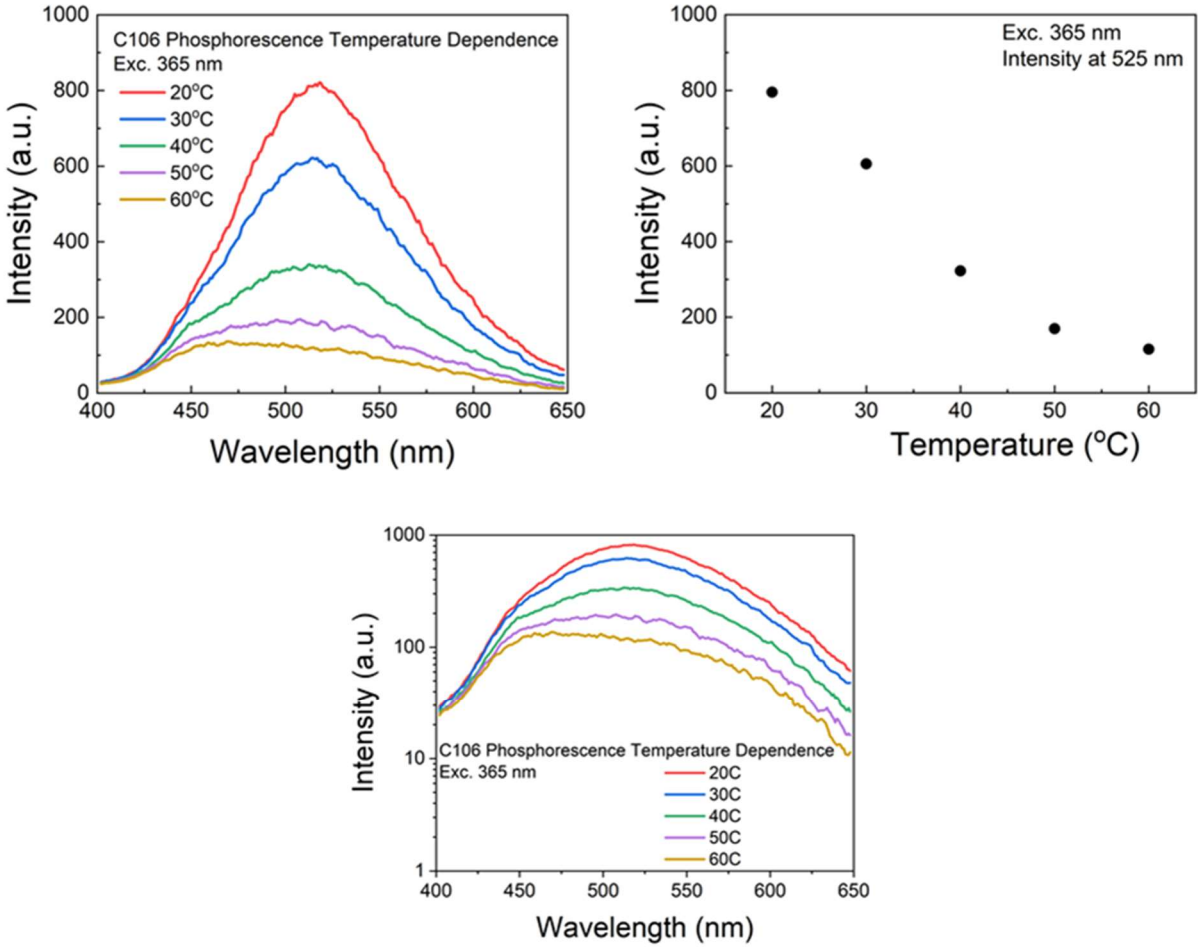

Figure 44. Temperature dependence of C106 in PVA film with 365 nm excitation. Top Left: spectra, top right: Intensities at 525 nm observation. As the temperature of the environment increases the phosphorescence of C106 in PVA film decreases. Bottom: spectra with log(Intensity) y axis.

The direct triplet excitation at 465 nm results in similar changes in the measured intensities, see Figure 45. However, long wavelength excitation induces very little delayed fluorescence, much less than UV excitation. This suggests that the reversed intersystem crossing transition ($T_1 - S_1$) occurs before or in time of an internal conversion in T_1 state. Looking at the logarithmic scale of the intensity to see if there was a shift in the peak wavelength as the temperature changed, a very slight red shift is revealed in the peak in the 500- 550 nm range as temperatures increase, and a plateau due to delayed fluorescence is found at 430 nm exists for all temperatures.

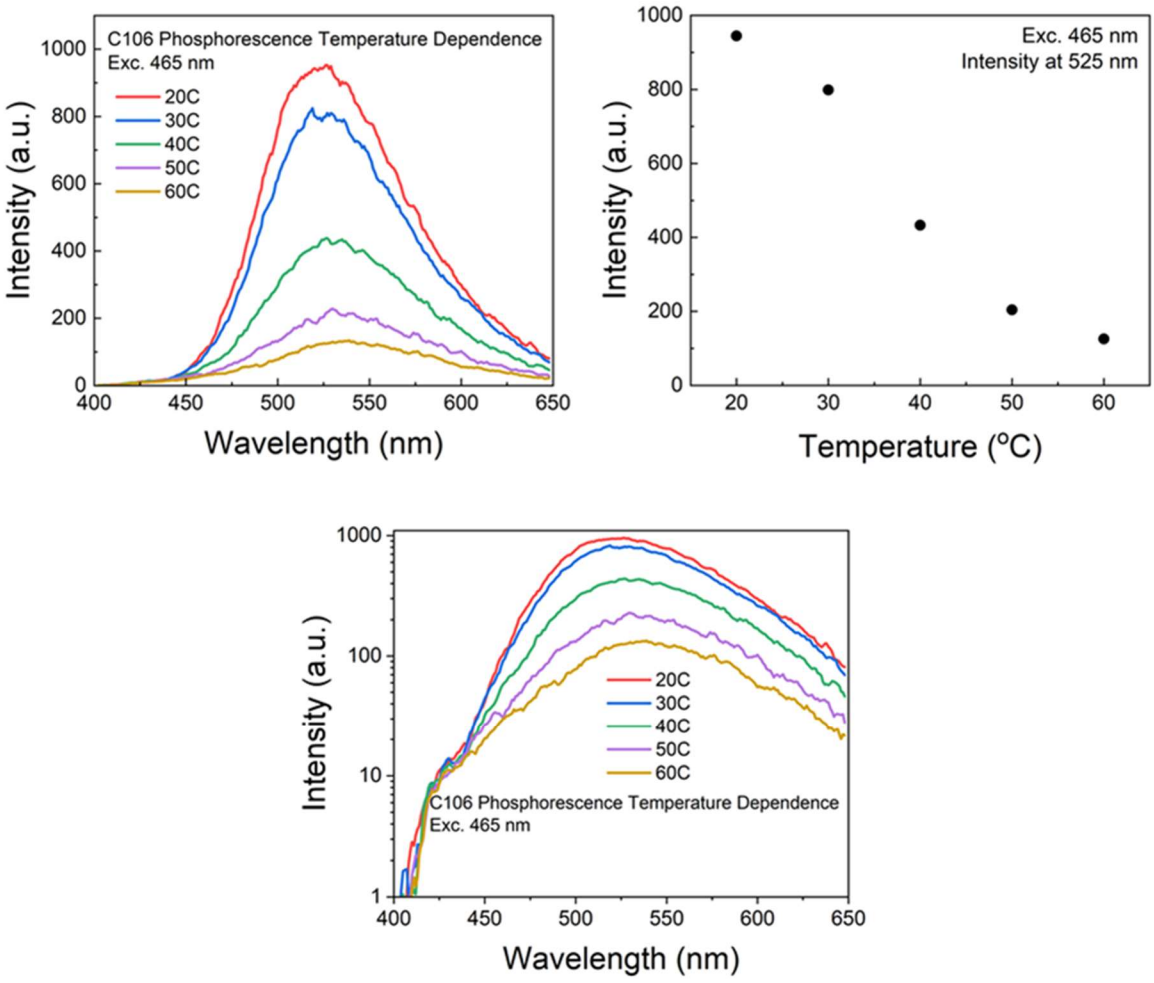

Figure 45. Temperature dependence of C106 in PVA film with 465 nm excitation. Top Left: spectra, top right: Intensities at 525 nm observation. As the temperature of the environment increases, the phosphorescence of C106 in PVA film decreases. Bottom: spectra with log(Intensity) y axis.

Based on other annealing reports [109-117] and what our annealed data had told us, C106 would show an improved RTP. Indeed, the phosphorescence intensity of annealed C106 in PVA film shows a significant increase, see Figure 46. The measurement was done with 405 nm excitation within the absorption band. The 405 nm excitation results in a residual delayed fluorescence (DF) already observed (Figures 43 and 44). Contrary to phosphorescence, the Delayed Fluorescence does not depend strongly on annealing. The phosphorescence backgrounds from both annealed and non-annealed samples (dashed lines) are negligible.

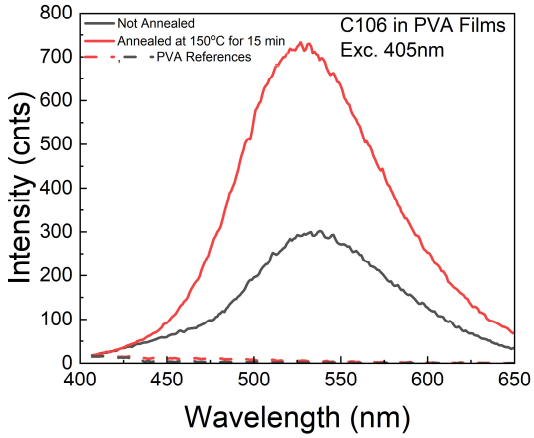

Figure 46. Phosphorescence emission spectra of C106 in PVA film with 405 nm excitation. Not annealed (black) and annealed for 15 minutes at 150 °C (red). There are PVA blank films taken as references (dashed lines).

The long-wavelength excitation (475 nm) of C106 in PVA samples is shown in Figure 47. Compared to 405 nm excitation, the effect is even stronger.

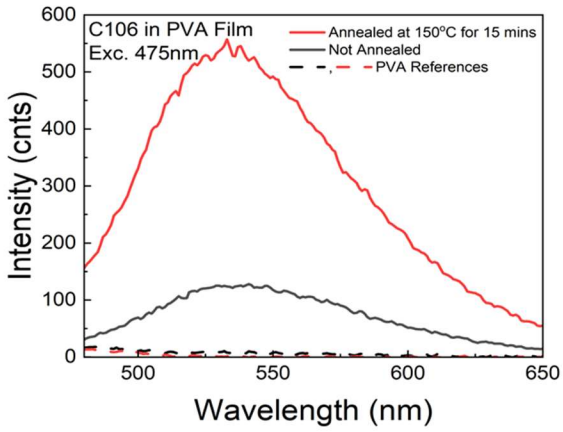

Figure 47. Direct triplet phosphorescence emission spectra of C106 in PVA film with 475 nm excitation. Not annealed (black) and annealed for 15 minutes at 150 °C (red). There are PVA blank films taken as references (dashed lines).

The strong effect of annealing increasing the phosphorescence of the samples prompted an investigation into the function of phosphorescence intensity over different annealing times. The effect was a many-fold enhancement at both 405 nm and 475 nm excitation; see Figures 48 and 49.

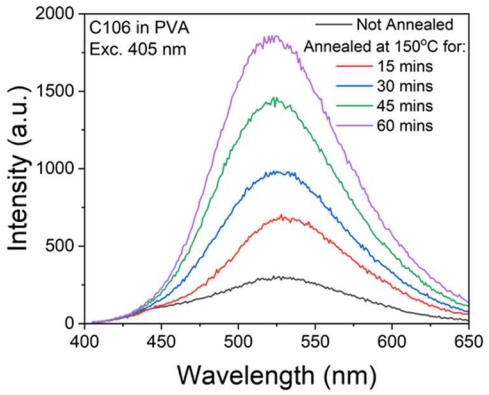

Figure 48. Effect of annealing on the phosphorescence of C106 in PVA films. The strips of PVA films doped with C106 were heated at different times at 150 °C. The excitation was at 405 nm, within the C106 absorption band. The not-annealed film (black) is at the bottom, with intensity increasing at each time interval, with 60 minutes (purple) being the highest phosphorescence intensity.

At 405 nm excitation, the phosphorescence spectra have been corrected for inner filter effects due to PVA absorptions as described in [46, 143-144].

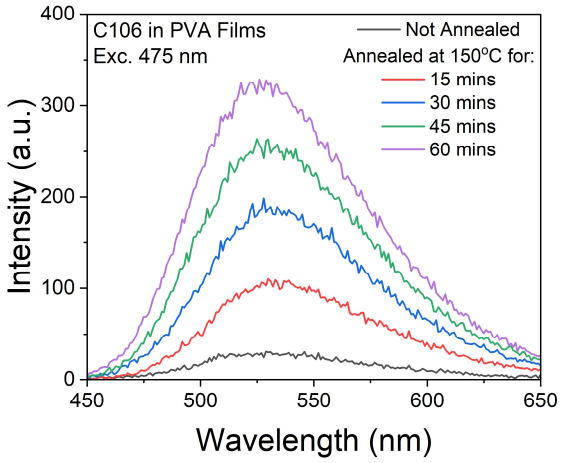

Figure 49. Effect of annealing on the phosphorescence of C106 in PVA films. The strips of PVA films doped with C106 were heated at different times at 150 °C. The excitation was at 475 nm. The not-annealed film (black) is at the bottom, with intensity increasing at each interval, with 60 minutes (purple) being the highest phosphorescence intensity.

No corrections for inner filter effects were needed with 475 nm excitation.

Anisotropy

The fluorescence anisotropy is high, slightly decaying over the redder wavelengths. Figure 50 shows the G-factor corrected spectra with the anisotropy overlaid on top. The excitation wavelength of the measurement was 375nm.

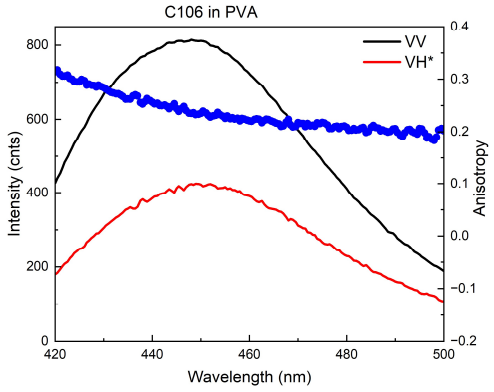

Figure 50.Fluorescence emission anisotropy (blue dots) of C106 in PVA film. The excitation wavelength was 375 nm. Black line- VV is a vertically polarized excitation and emission. Red line- VH is a vertically polarized excitation, horizontal emission, and the * implies it has been G-factor corrected. Anisotropy is high and positive.*

The phosphorescence excitation anisotropy spectrum, Figure 51, shows a transition from low/negative anisotropy in the UV region to high positive in the blue region. The phosphorescence anisotropy with the long wavelength excitation is as high as fluorescence anisotropy (Figure 50).

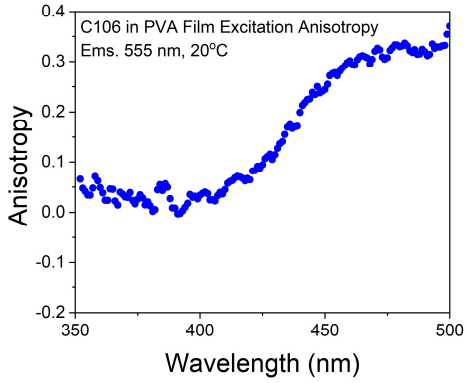

Figure 51. Phosphorescence excitation anisotropy spectrum of C106 in PVA film. Figure 28, the legend, and the Material and Methods section describe the parameters used for the gated detection.

This suggests that the singlet-triplet transition (absorption) is parallel to the triplet–singlet transition (phosphorescence).

The phosphorescence emission anisotropy measured with a 475 nm excitation wavelength is steady across the emission spectrum, see Figure 52. The VH (vertically polarized excitation and emission observed through a horizontally oriented polarizer) component of phosphorescence emission was corrected for the G-factor of the spectrofluorometer, Figure 52, red). Such long-wavelength excitation of RTP results in a lower background (Figure 47) but also higher anisotropy, see Figure 52.

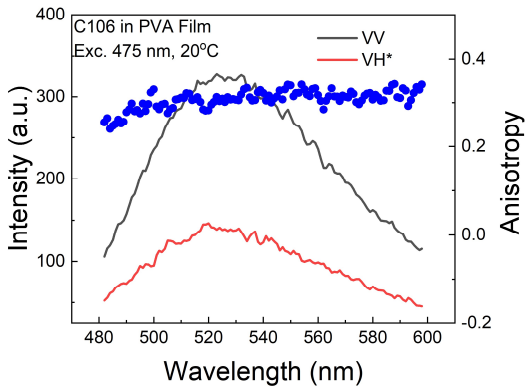

Figure 52. Phosphorescence emission anisotropy spectrum of C106 in PVA film. Figure 28, the legend, and the Material and Methods section describe the parameters used for the gated detection. VV is vertically polarized excitation and emission, black line. VH is vertical polarized excitation, horizontal emission, and the * implies it has been G-factor corrected (red line). Anisotropy is high and positive.*

We checked if annealing affects fluorescence anisotropy. The measurements of fluorescence emission anisotropies for not annealed and annealed samples are shown in Figure 53.

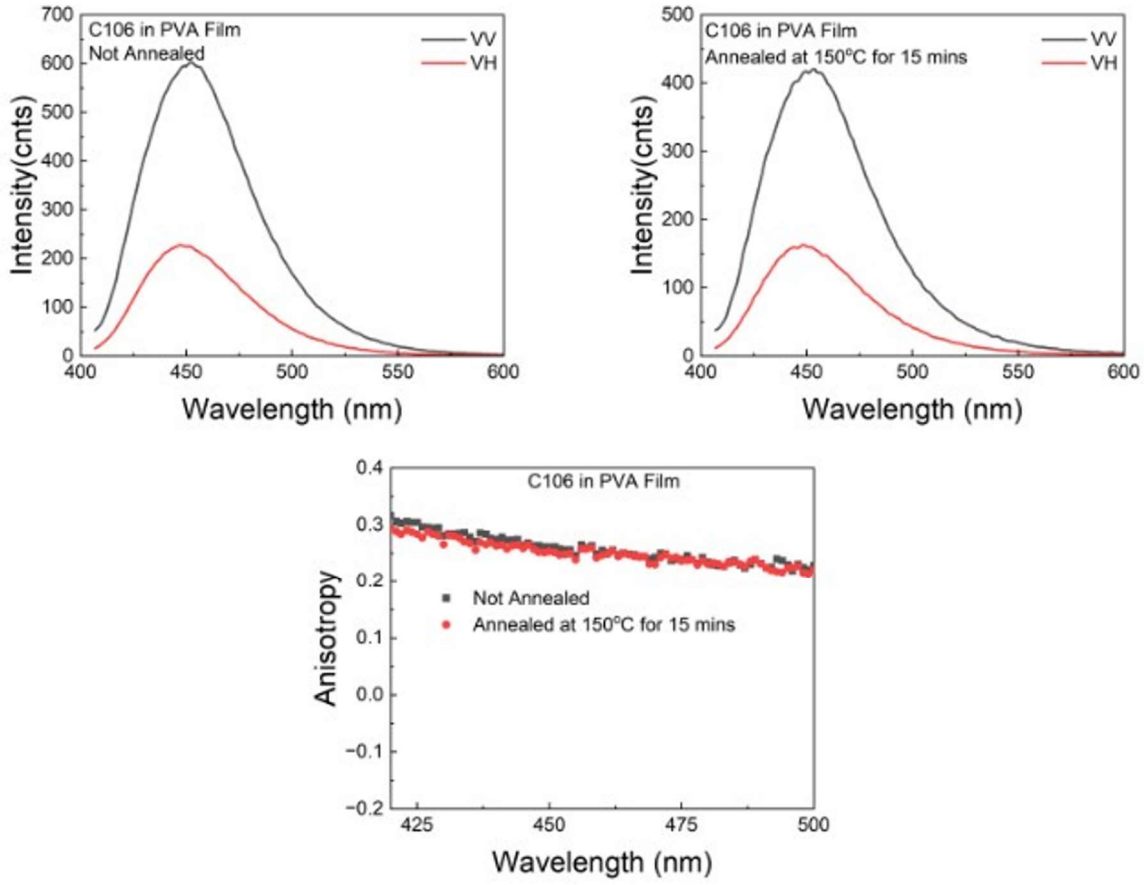

Figure 53 Top: Polarized components of C106 in PVA films fluorescence emission of not annealed (left) and annealed sample at 150^{O}C for 15 min. Bottom: Fluorescence anisotropy of C106 in PVA films: not annealed (black) and annealed at 150^{O}C for 15 minutes.

Evidently, anisotropies are not affected by the annealing process. However, it must be noted that PVA strips cannot be placed between rigid surfaces (like glass slides) and squeezed in annealing, and the cooling cannot be rapid. Not carefully performing the annealing process may result in PVA residual crystallization, and these areas become optically active (rotate the plane of light polarization). However, not-squeezed and slowly cooled down remain amorphic, see Figure 54.

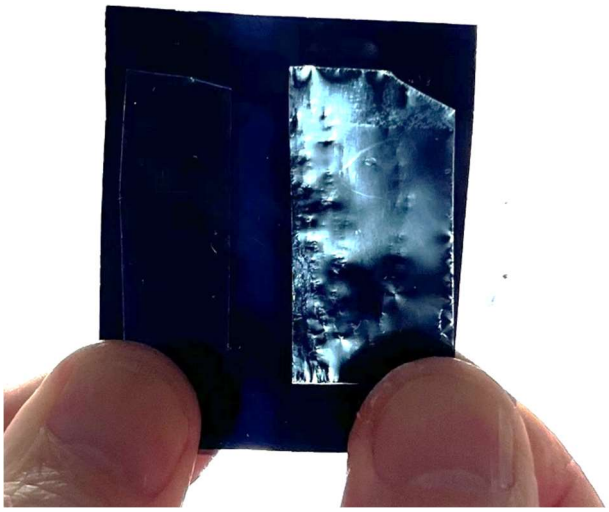

Figure 54. Two PVA polymer strips between crossed polarizers. Left: Carefully annealed for 15 minutes at 150^{O}C and slowly cooled down; Right: Squeezed between glass slides during 15 minutes of annealing and rapidly cooled.

Figure 55 is the excitation spectra of C106 annealed for 15 minutes at 150 °C. The excitation to S_1 state results in a very low/negative phosphorescence anisotropy because T_1 state (populated by the inter-system crossing process) is orthogonal to the singlet. In the case of direct triplet state excitation, the phosphorescence anisotropy is high, just like for fluorescence.

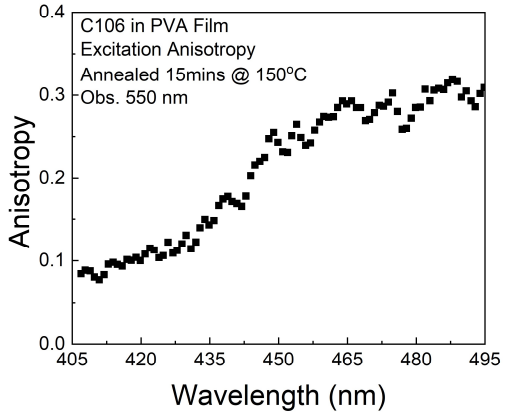

Figure 55. Phosphorescence excitation anisotropy of C106 in PVA film annealed at 150 °C for 15 min.

All the abovementioned measurements were done with the same pair of not-annealed/annealed samples and their references.

Quantum Yield

We compared the fluorescence emission of C106 in PVA film not annealed and QS in 1NH2SO4. The concentration of QS was adjusted so that its absorbance matched the absorbance of the not annealed C106 in PVA film at 375 nm, see Figure 56.

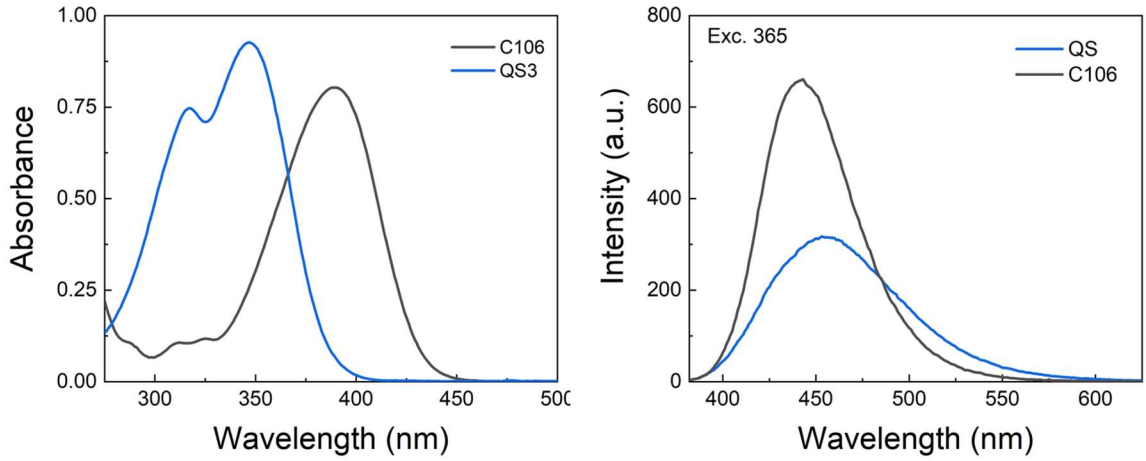

Figure 56. Absorption (left) and fluorescence (right) spectra of C106 in PVA and QS reference.

At the excitation of 375 nm, the optical density (OD) of the C106 was 0.581, and the optical density of the QS reference was 0.535.

The integrated fluorescence intensity of C106 in PVA film at 375 nm excitation is 41816 (a. u.) and 27896 (a. u.) for QS, which gives the ratio of $(I\ /\ I_R)$ = 1.499. The refractive indexes of PVA and 1N H2SO4 are 1.50 and 1.35, respectively, and Q_R = 0.546 [145]. The QY of C106 in PVA is 0.97.

Time-Resolved Measurements

The Fluorescence lifetime of C106 in PVA film was measured to be a single decay with a lifetime of 4.92 ns, Figure 57.

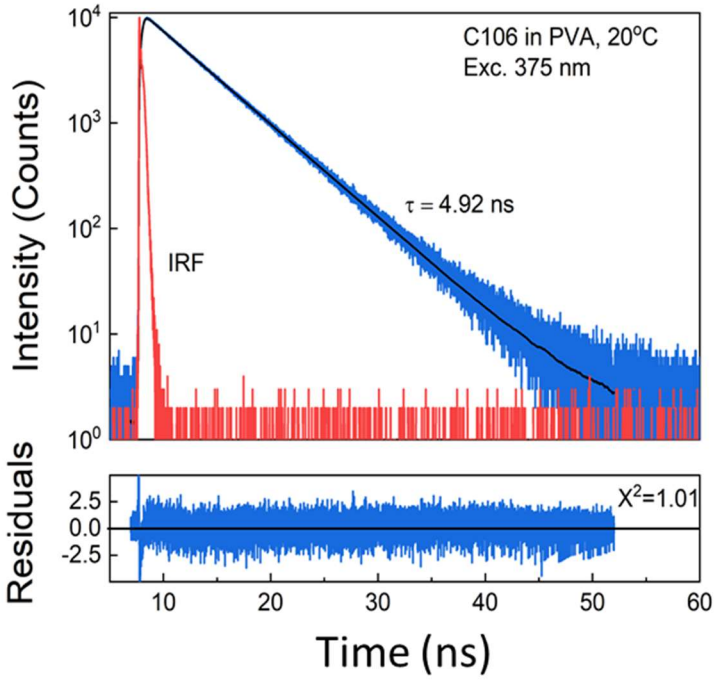

Figure 57. Fluorescence intensity decay of C106 in PVA film not annealed analyzed with single exponent. The measurement was performed with an excitation of 375 nm and observation of 540 nm. IRF is in red, measured intensity decay is black, and the model is in blue. The lifetime, $\tau = 4.92ns$ *with a* $\chi^2 = 1.01$.

Lifetimes of C106 in PVA samples have only a slight decrease in the lifetime as the annealing time of the samples increase, see Figure 58. Both the fluorescence intensity and lifetime measurements suggest that deactivation processes increase in annealed samples (absorptions change is insignificant).

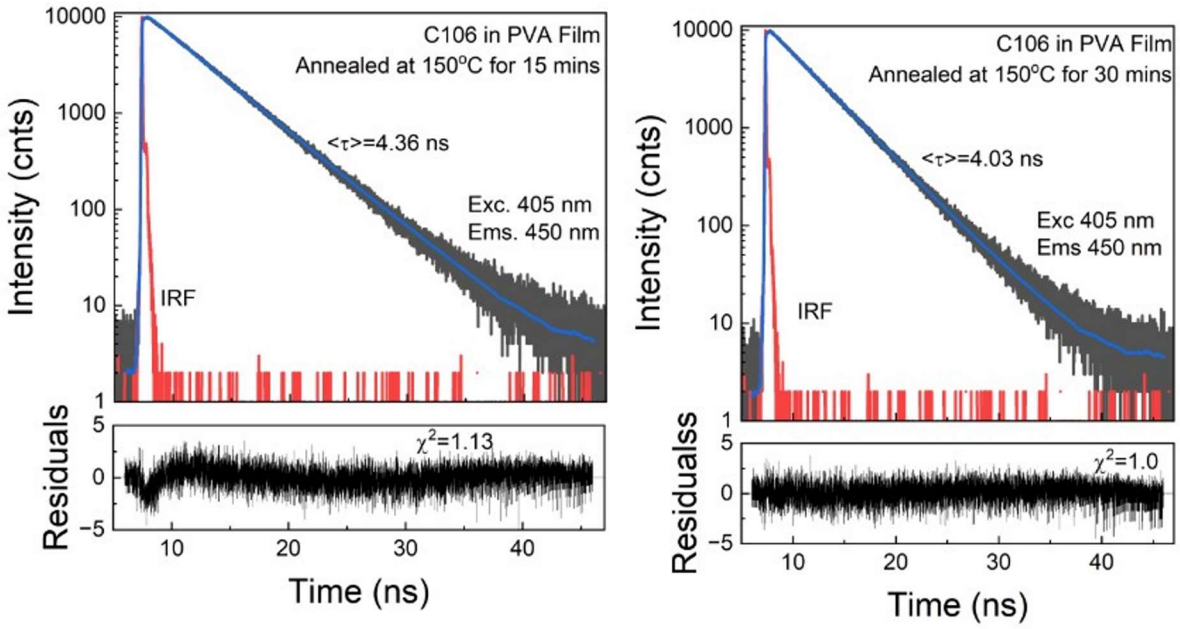

Figure 58. Fluorescence intensity decay of C106 in PVA film not annealed analysed with single exponent. The measurements were performed with an excitation of 405 nm and an observation of 450 nm. IRF is in red, measured intensity decay is black, and the model is blue. Fluorescence intensity decays of C106 in PVA films annealed at 150°C for 15 min (left) and 30 min (right).

Phosphorescence intensity decays of C106 in PVA films are complex and but can still be fitted satisfactorily, see Figures 59 and 60.

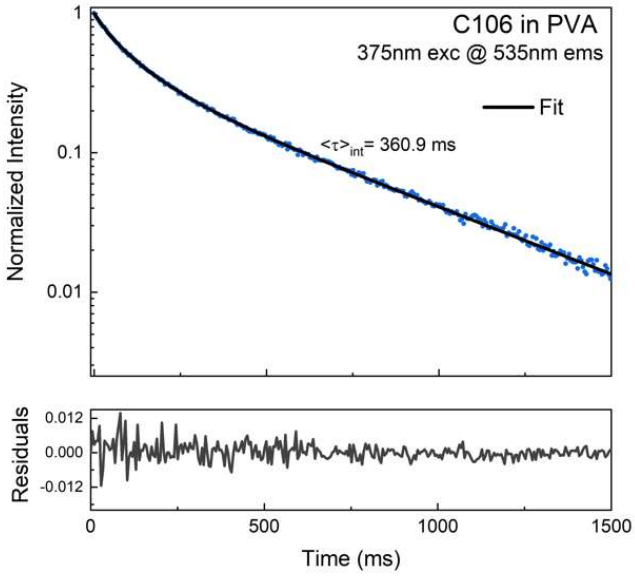

Figure 59. Phosphorescence intensity decay of C106 in PVA film excited at 375 nm and observed at 535 nm. Gating parameters are described in the Materials and Methods section and Figure 28 legend.

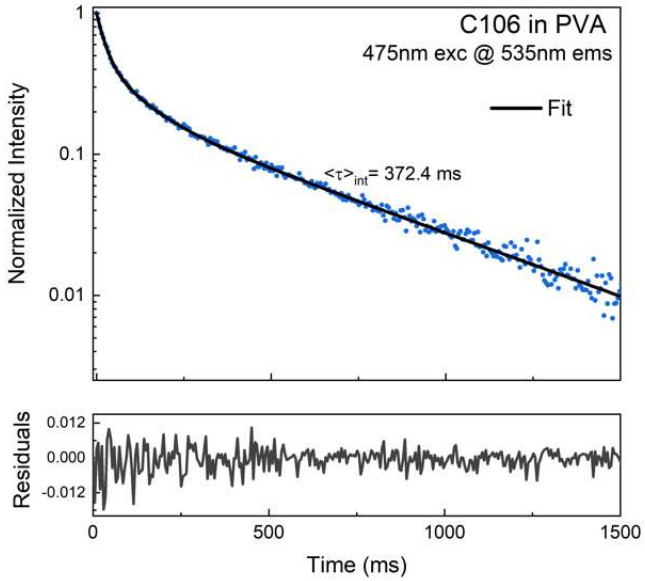

Figure 60. Phosphorescence intensity decay of C106 in PVA film excited at 375 nm and observed at 535 nm. Gating parameters are described in the Materials and Methods section and Figure 28 legend.

However, the lifetime of the annealed samples is shorter at 132 $\pm$ 5 ms, see Figure 61. The phosphorescence intensity increases proportionally, as shown in Figure 48. A simultaneous increase in intensity and decrease in a lifetime has been observed in metal-enhanced fluorescence [130] and explained by a modification of the radiative decay rate (called radiative decay engineering). In the case of annealing, we believe that the radiative rate increases also due to stronger spin-orbit interactions. The decrease in the nonradiative rate would result in an increased lifetime.

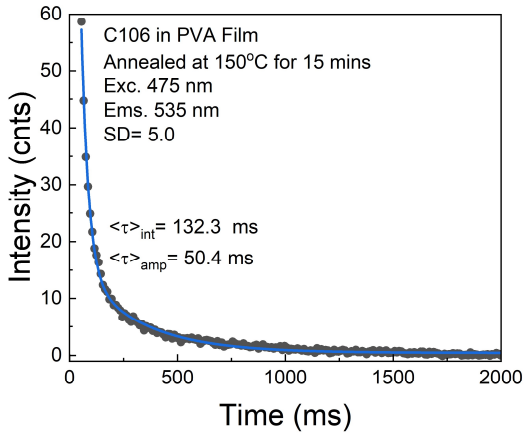

Figure 61. Phosphorescence intensity decay of C106 in PVA film annealed for 15 minutes at 150^{O} C. The decay can be satisfactorily fitted to a bi-exponential model with the parameters: α_1 = 229 $\pm$ 15, τ_1 = 33 $\pm$ 3 ms, : α_2 = 17 $\pm$2 and τ_2 = 282 $\pm$ 8 ms, and a standard deviation of 5.0.

RTP Enhancement without Absorption Alteration

Finally, we investigated the case where annealing did not affect the absorption of PVA in the UV range. Looking back at Figure 31, annealing at 110 °C practically does not change PVA absorption. With fresh samples, we annealed the samples at 110°C for 30 mins and then repeated the experimental measurements (absorption, fluorescence, and phosphorescence).

When annealing at 110 °C for 30 minutes, we found the absorbance has a minimal change in both the C106 and UV PVA peaks, see Figure 62.

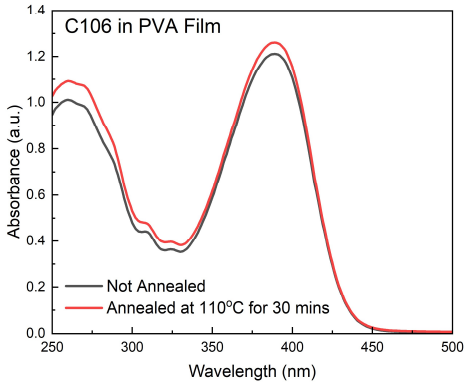

Figure 62. Absorption of C106 in PVA films: not annealed (black) and annealed for 30 min at 110 °C (red).

When looking at the fluorescence spectra, we see there is not a significant decrease in the fluorescence spectra when annealed at 110 °C for 30 minutes as compared to the not annealed spectra, see Figure 63.

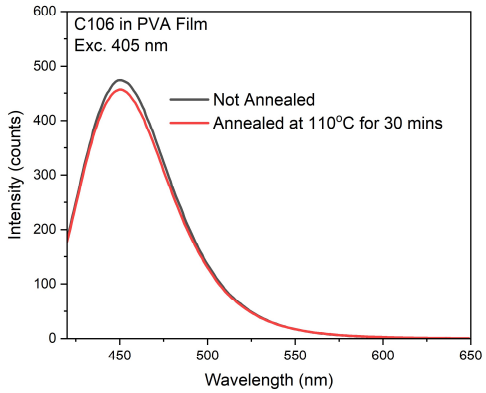

Figure 63. Fluorescence of C106 in PVA films: not annealed (black) and annealed for 30 min at 110^{O} C (red).

The phosphorescence intensity of annealed C106 in PVA film shows a significant increase, see Figure 64. The measurement was done with 405 nm excitation within the absorption band. The phosphorescence backgrounds from both annealed and non-annealed samples (dashed lines) are negligible.

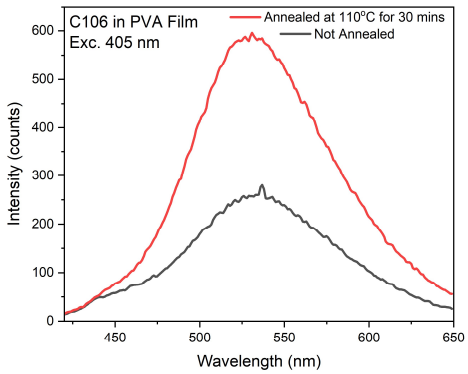

Figure 64. Phosphorescence of C106 in PVA films: not annealed (black) and annealed for 30 min at 110^{O} C (red) at 405nm excitation.

The long-wavelength excitation (475 nm) of C106 in PVA samples is shown in Figure 65.

Compared to 405 nm excitation, the effect is even stronger.

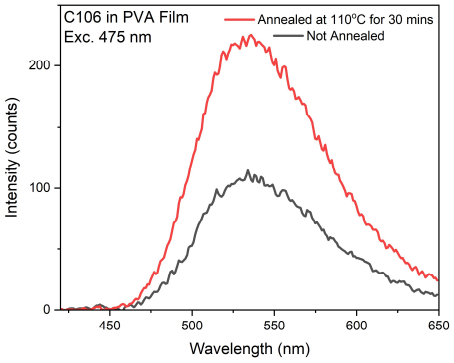

Figure 65. Phosphorescence of C106 in PVA films: not annealed (black) and annealed for 30 min at 110^{O} C (red) at 475nm excitation.

The phosphorescence excitation spectrum of C106 in PVA film differs from the fluorescence excitation spectrum. When annealing is applied to the C105 in PVA film at 110 °C for 30 minutes, we find an increase in the signal above 420 nm; see Figure 66. At longer wavelengths, the triplet state T_1 of C106 has been directly excited, and the excitation spectra show that annealing the sample further increases the phosphorescence signal.

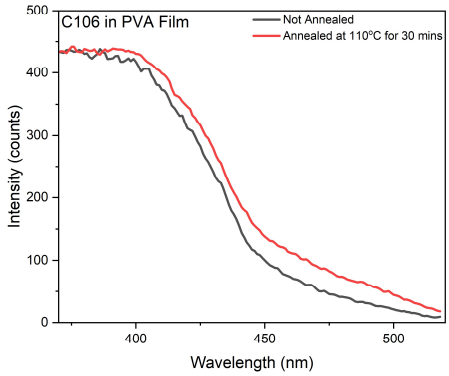

Figure 66. Phosphorescence excitation spectra of C106 in PVA films: not annealed (black) and annealed (red) for 30 min at 110^{O} C.

From this, we conclude that annealing promotes phosphorescence excitation at longer wavelengths. Moreover, about 100% enhancement in phosphorescence intensity can be achieved without altering PVA absorption.

Conclusion

For this thesis, we set out to investigate further the use of PVA film to enhance the phosphorescence (RTP) of the chromophore embedded in the sample. Our work had previously been on investigating indole and indole derivatives [19, 36-38] and a few chromophores [39-40] in PVA film. However, in our previous work, there was no further investigation into the SOC of the system or if further SOC enhancement could be performed. Our work using DAPI and C106 in PVA film (separately) looked to start the research into how to capitalize on the PVA film immobilization and further enhance the RTP of organic chromophores [41, 118-119]. This is done with the ultimate long-term goal of getting the RTP of liquid samples. Below we summarize the answers to the questions posed for this thesis.

1. Characterize the photophysical properties of DAPI in PVA film and C106 in PVA film. Can RTP be distinguishably detected in measurements on these films?

We were able to characterize the photophysical properties of DAPI in PVA film.

DAPI in PVA film has an absorbance maximum at 360 nm, Figure 10, and a fluorescence maximum of 425 nm, Figure 11. We did find the absorbance and fluorescence maximums to be shifted from the expected values of DAPI in water. However, further investigation (Figures 27 and 28) revealed a difference in the polarity between DAPI in water and DAPI in PVA film.

We can confirm that the RTP of DAPI in PVA film is measurable using UV excitation and was taken via a smartphone, see Figure 2. Using our UV excitation of 375 nm, we measured phosphorescence emission spectra with a peak at 550 nm, Figure 13. Further analysis of the phosphorescence spectra revealed a component of the spectra that can be attributed to the delayed fluorescence of DAPI in PVA film, Figure 14.

The fluorescence anisotropy is high, around 0.3, and steady, which is expected using PVA film as an immobilizer, Figures 17 and 18. The phosphorescence anisotropy with UV excitation is negative, -0.1, corresponding to the anisotropy values expected when ISC is the main pathway of phosphorescence emission.

The fluorescence QY is found to be above 70%, and the phosphorescence QY using 375 nm excitation is found to be about 0.09%.

Furthermore, we ran the fluorescence lifetimes of DAPI in PVA and found a mono-exponential fit with a lifetime of 2.2 ns, Figure 25. The phosphorescence lifetime when using UV excitation is a mono-exponential fit with a lifetime of 323 ms, Figure 26.

After sufficiently characterizing the photophysical properties of DAPI in PVA film and confirming that we can indeed detect and measure the phosphorescence of DAPI in PVA film, we investigated C106 in PVA film.

C106 in PVA film has a maximum absorbance of 370 nm, Figure 29. The fluorescence maximum of C106 in PVA film using 365 nm excitation is 450 nm, Figure 34.

Figure 3 confirmed the existence of phosphorescence when using a UV illuminator. Using UV excitation (365 nm), we measured a phosphorescence peak at about 540 nm, Figure 42. The UV phosphorescence measurement also included some measurable delayed fluorescence, and we decovolved the spectra in Figure 42.

The fluorescence anisotropy of C106 in PVA film is high, although it decreases slightly (from 0.3 to 0.2). The phosphorescence excitation anisotropy is low, not quite negative in the UV range, Figure 51. This indicates that both ISC and possibly some direct triplet state excitation occur in the UV range. We found the fluorescence QY of C106 in PVA film to be very high, at around 97%.

The fluorescence lifetime of C106 in PVA film is a mono-exponential fit with a lifetime of about 4.92 ns, Figure 57. The UV excitation (375 nm) phosphorescence lifetime is also mono-exponential with a lifetime of about 360 ms, Figure 59.

2. Can we directly excite the phosphorescence of the DAPI and C106 films and avoid the traditional ISC route?

With the confirmation of the existence of RTP for DAPI in PVA film, we investigated the possibility of directly exciting the triplet excited state. Figure 12 compares the fluorescence and phosphorescence excitation spectra, and starting at 420 nm, the intensity of the phosphorescence excitation spectra supersedes the intensity of the fluorescence spectra.

Using 455 nm excitation, we detected phosphorescence emission via direct triplet state excitation on the Varian Eclipse, Figure 15. The phosphorescence peak is still 550 nm, and we detected a much stronger signal using a 488 nm laser and an Ocean Optics (CCD) spectrometer.

The phosphorescence anisotropy in the blue excitation range (420 nm and above) is high and positive in Figure 20. This tells us that ISC is not the main activation path of the phosphorescence in these ranges, and instead, the direct triplet excitation is the main activation path. These results conclude that direct triplet state excitation is possible for DAPI in PVA film.

2b. Now investigating into C106 in PVA. Can we directly excite the phosphorescence by directly exciting the triplet state?

Analyzing the phosphorescence excitation spectra of Figure 38, we find that the excitation spectra are vastly different from the absorbance spectra, see Figure 40. This suggests that the triplet state is not only populated via ISC. C106 in PVA film can also be excited well outside the possible

absorbance range above 450 nm. Indeed, when excited with 465 nm (blue excitation), we found phosphorescence spectra with a maximum of 540 nm, the same as the UV excitation, Figure 43.

The phosphorescence excitation anisotropy is high, about 0.3, at 450 nm and above, Figure 51. Looking at phosphorescence emission anisotropy using 475 nm excitation, we find the anisotropy to be high and positive (0.3), as shown in Figure 52. The high and positive values for the phosphorescence anisotropies when using blue excitation indicate that direct triplet excitation is the main source of phosphorescence.

The phosphorescence lifetime using 475 nm excitation is 372 ms, Figure 60, only slightly higher than the reported phosphorescence of the UV excitation (summarized in question 1).

3. Using C106 in PVA film, can we alter the phosphorescence with the effects of annealing to produce a greater signal?

When performing annealing on the C106 in PVA films, we found that not only can we alter the phosphorescence detection, but annealing at 150°C also altered the PVA film that C106 is in.

In Figure 30, we measured the absorbance of C106 in a PVA film and a blank PVA film, which were both annealed for 15 minutes at 150°C and compared to the absorbances of the not annealed films. We found that the PVA film itself significantly increases absorbance in the UV range, but with careful subtraction, we can recover a C106 spectrum that does not change due to annealing. Further investigation into the changing of PVA film via annealing was performed (Figures 31 through Figure 33). We were able to confirm that the temperature of annealing and the length of annealing affect the absorbance of the PVA film itself but not the C106 in the film.

For fluorescence studies, we found that changing the environmental temperature of not annealed C106 in PVA film does not change the fluorescence signal, Figure 35. This is expected of

fluorescence measurements [46, 70-71]. For fluorescence of the annealed samples compared to the not annealed samples, we found that at 150°C, there is a significant decrease in fluorescence between the not annealed sample and the annealed for 15 minutes sample, followed by another significant decrease in fluorescence between the annealed for 15 minutes sampled and the annealed for 30 minutes sample. By comparing the decrease in fluorescence at 150°C to other temperatures (Figure 37) one finds that the decrease at 150°C is larger than the other temperatures used (110°C, 120°C, and 135°C).

For the temperature studies of phosphorescence, we looked at the effect of the environment temperature for both UV and Blue excitation, Figures 44 and 45. In both cases, we found that as the temperature of the environment increases from 20 $°C$ to 60$°C$, the phosphorescence decreases. This is to be expected of phosphorescence, which is why RTP is difficult to see without matrix immobilization. For the annealed sample of C106 in PVA film, Figures 46 and 47, we find that with both the UV and the blue excitation, there is a significant increase in the phosphorescence signal when the films are annealed. From the phosphorescence measurements of the samples annealed at 150°C over increasing times from 15 to 60 minutes, Figures 48 and 49, wee found that the longer the sample is annealed, the greater is the increase in the phosphorescence signal for both the UV and blue excitations.

From the fluorescence anisotropy experiments, we found that there was no difference in the anisotropy measurements between the annealed and not annealed samples, Figure 53. Both anisotropies are high and only slightly drop, from 0.3 to 0.2. The phosphorescence excitation anisotropy of the annealed samples changes from low (almost negative) to high, indicating a region in which the annealed sample can be excited via direct triplet state excitation, Figure 55.

However, we found that using enhancement techniques like annealing can come at a cost. Without careful attention to how the sample is cooled, there is a risk of the loss of the isotropic property of the film before treatment. Heated films become optically active and rotate the light polarization, Figure 54. Careful measurements should be performed to determine if such films should or should not be used for anisotropy measurements.

For annealed samples, we found minimal changes in the fluorescence lifetimes, with a slight decrease from 4.92 ns not annealed, to 150°C at 15 minutes, 4.36 ns, to 150°C at 30 minutes, 4.03 ns, Figures 57 and 58. The lack of change is expected with the fluorescence lifetimes of our samples as they are relatively immobile in the PVA film. However, for the phosphorescence, the lifetime of not annealed samples at 372 ms drops, when the sample is annealed, to a lifetime of 132 ms, Figures 60 and 61. The increase in intensity but a decrease in lifetime and has been seen before in metal enhanced fluorescence [130]. This is due to a modification of the radiative decay rate (called radiative decay engineering). In our case, we believe the radiative rate also increases due to stronger spin-orbit interactions. The decrease in the nonradiative rate would result in an increased lifetime, see Equation 22.

Lastly, the lack of change in the PVA absorbance spectra between the not annealed sample and the sample annealed at 110°C (Figure 31) prompted us to investigate whether we can obtain phosphorescence enhancement without changing the absorbance of PVA. When annealing at 110°C for 30 minutes, we found a minimal change in absorbance of the C106 in PVA film as compared to the not annealed sample, Figure 62. In the fluorescence spectra, we found no significant decrease in the fluorescence signal from the not annealed sample to the annealed sample, unlike what we saw with the 150°C annealing. But even with the lack of change in absorbance and fluorescence between the not annealed and annealed samples, we found that the

phosphorescence signal of the annealed sample still increases by about 100% when with UV and blue excitation, compared to the not annealed sample, Figures 64 and 65. Lastly, for the phosphorescence excitation, Figure 66; the annealed sample has a further increase in the signal above 420 nm. This indicates that at longer wavelengths, the triplet state T_1 of C106 in PVA film can be directly excited.

4. Looking towards the future of RTP of liquid samples, what can we conclude, if anything, about external perturbations?

Our recent work delved into immobilizing luminophores into PVA film [19, 36-41, 118-119]. This thesis focuses on the SOC perturbation of DAPI in PVA film and C106 in PVA film [41, 119]. We have begun investigating the enhancement of the SOC perturbation of PVA film using external perturbations [118], where we investigated the use of annealing on PVA films.

Following our work, we have preliminary data on investigating other external perturbations of luminophores in PVA films. We have results for 4-Methylumbelliferone (4MU) in PVA film that indicate a change in pH might affect the enhancement of phosphorescence, Figure 67.

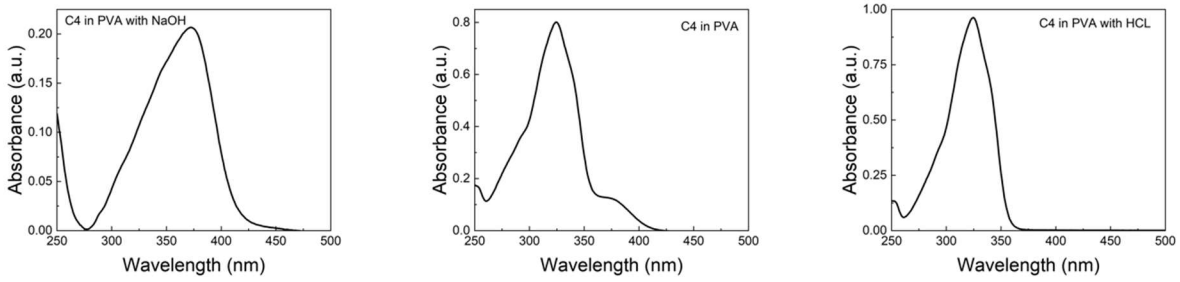

Figure 67. The absorbance of 4MU in PVA film when mixed with different pH values. Left: the absorbance spectra of 4MU in PVA with NaOH (basic pH); middle: the absorbance spectra of 4MU in PVA with neutral pH; right: the absorbance of 4MU in PVA with HCL (acidic pH).

Our long-term future work goal is to look into the external perturbation of SOC in liquid solutions.

References

[1] Yang J, Fang M and Li Z 2425 Stimulus-responsive room temperature phosphorescence materials: internal mechanism, design strategy, and potential application Accounts of Materials Research. 2 644-54

[2] Hackney H E and Perepichka D F 2426 Recent advances in room temperature phosphorescence of crystalline boron containing organic compounds: Nanoscience: Special Issue Dedicated to Professor Paul S. Weiss Aggregate. 3 e127

[3] Feng R, Wang M, Zhang Z, Hu P, Wu Z, Shi G, Xu B, Liu H, and Ma L-J 2427 Polymer-Based Long-Lived Phosphorescence Materials over a Broad Temperature Based on Coumarin Derivatives as Information Anti-Counterfeiting ACS Applied Materials & Interfaces. 15 34721-30

[4] Gao R, Yan D, Evans D G and Duan X 2421 Layer-by-layer assembly of long-afterglow self-supporting thin films with dual-stimuli-responsive phosphorescence and antiforgery applications Nano Research. 10 4006-21

[5] Su Y, Phua S Z F, Li Y, Zhou X, Jana D, Liu G, Lim W Q, Ong W K, Yang C and Zhao Y 2422 Ultralong room temperature phosphorescence from amorphous organic materials toward confidential information encryption and decryption Science Advances. 4 eaas9736

[6] Sánchez-Barragán I, Costa-Fernández J, Sanz-Medel A, Valledor M and Campo J 2406 Room-temperature phosphorescence (RTP) for optical sensing TrAC Trends in Analytical Chemistry. 29 958-67

[7] Xiao F, Gao H, Lei Y, Dai W, Liu M, Zheng X, Cai Z, Huang X, Wu H and Ding D 2426 Guest-host doped strategy for constructing ultralong-lifetime near-infrared organic phosphorescence materials for bioimaging Nature Communications. 13 226

[8] Si C, Wang T, Gupta A K, Cordes D B, Slawin A M, Siegel J S and Zysman-Colman E 2427 Room-Temperature Multiple Phosphorescence from Functionalized Corannulenes: Temperature Sensing and Afterglow Organic Light-Emitting Diode Angewandte Chemie International Edition. 62 e242749722

[9] Ji M and Ma X 2427 Recent progress with the application of organic room-temperature phosphorescent materials Industrial Chemistry & Materials. 1 582-94

[10] El-Sayed M and Brewer R 2363 Polarization of the $\pi^* \rightarrow \pi$ and $\pi^* \rightarrow n$ Phosphorescence Spectra of N-Heterocyclics The Journal of Chemical Physics. 39 2027-8

[11] Lim E and Yu J M 2367 Vibronic Spin—Orbit Interactions in Heteroaromatic Molecules. I. Polycyclic Monoazines The Journal of Chemical Physics. 47 3670-5

[12] McGlynn S P, Azumi T and Kinoshita C 2369 Molecular spectroscopy of the triplet state (Englewood Cliffs, New Jersey, United States of America: Prentice-Hall).

[13] Lewis G N, Lipkin D and Magel T T 2341 Reversible photochemical processes in rigid media. A study of the phosphorescent state Journal of the American Chemical Society. 63 3405-22

[14] Kuijt J, Ariese F, Udo A and Gooijer C 2403 Room temperature phosphorescence in the liquid state as a tool in analytical chemistry Analytica chimica acta. 488 139-71

[15] Gong Y, Tan Y, Mei J, Zhang Y, Yuan W, Zhang Y, Sun J and Tang B Z 2413 Room temperature phosphorescence from natural products: Crystallization matters Science China Chemistry. 56 1218-82

[16] Yuan J, Zhai Y, Wan K, Liu S, Li J, Li S, Chen Z and James T D 2425 Sustainable afterglow materials from lignin inspired by wood phosphorescence Cell Reports Physical Science. 2 100542

[17] Luo X, Tian B, Zhai Y, Guo H, Liu S, Li J, Li S, James T D and Chen Z 2427 Room-temperature phosphorescent materials derived from natural resources Nature Reviews Chemistry. 7 800-12

[18] Gong Y, Yang J, Fang M and Li Z 2426 Room-temperature phosphorescence from metal-free polymer-based materials Cell Reports Physical Science 3, 10105

[19] Chavez J, Kimball J, Ceresa L, Kitchner E, Shtoyko T, Fudala R, Borejdo J, Gryczynski Z, and Gryczynski I 2425 Luminescence properties of 5-Bromoindole in PVA films at room temperature: Direct triplet state excitation Journal of Luminescence. 274 121728

[20] Mukherjee, S. & Thilagar, P. Recent advances in purely organic phosphorescent materials. Chem. Comm. 51, 10988–11003 (2015).

[21] Svoboda, O., and P. Slavícek. Is Nitrate Anion Photodissociation Mediated by Singlet−Triplet Absorption? J. Phys. Chem. Lett. 5, 1958−1962, 2014.

[22] Xu, S., Chen, R., Zheng, C. & Huang, W. Excited state modulation for organic afterglow: materials and applications. Adv. Mater. 28, 9920–9940 (2016).

[23] Hirata, S. Recent advances in materials with room-temperature hosphorescence: photophysics for triplet exciton stabilization. Adv. Opt. Mater. 5, 1700116 (2017).

[24] Baroncini, M., Bergamini, G. & Ceroni, P. Rigidification or interaction induced phosphorescence of organic molecules. Chem. Comm. 53, 2081–2093 (2017).

[25] Forni, A., Lucenti, E., Botta, C. & Cariati, E. Metal free room temperature phosphorescence from molecular self-interactions in the solid state. J. Mater. Chem. C. 6, 4603–4626 (2018)

[26] Tao, Y., R. Chen, H. Li, J. Yuan, Y. Wan, H. Jiang, C. Chen, Y. Si, C. Zheng, B. Yang, G. Xing, W. Huang. Resonance-Activated Spin-Flipping for Efficient Organic Ultralong Room-Temperature Phosphorescence. Adv. Materials 30, 1803856, 2018.

[27] Yang, J., X. Zhen, B. Wang, X. Gao, Z. Ren, J. Wang, Y. Xie, J. Li, Q. Peng, K. Pu & Z. Li. The influence of the molecular packing on the room temperature phosphorescence of purely organic luminogens. Nature Communications 9, 840, 2018.

[28] Ren, J., Y. Wang, Y. Tian, Z. Liu, X. Xiao, J. Yang, M. Fang, Z. Li. Force-Induced Turn-On Persistent Room-Temperature Phosphorescence in Purely Organic Luminogen, Angewandte Chemie, 10.1002/ange.202101994, 133, 22, (12443-12448), (2021).

[29] Chen, C., & B. Liu. Enhancing the performance of pure organic room temperature phosphorescent luminophore. Nature communications 10.1 (2019): 1-15.

[30] Mengke Li,a Xinyi Cai,a Zijian Chen,a Kunkun Liu,a,b Weidong Qiu,a Wentao Xie,a Liangying Wanga and Shi-Jian Su. Boosting Purely Organic Room-Temperature Phosphorescence Performance through Host-Guest Strategy. Chem. Sci., 2021, 12, 13580-13587.

[31] W. Rothman, W., Case, A., Kearns, D. 1965. Determination of singlet-triplet absorption spectra from phosphorescence excitation spectra: α-bromonaphthalene. J. Chem. Phys. 43: 1067.

[32] Borkman, R. and Kearns, D. 1966. Investigation of singlet-triplet transitions by the phosphorescence excitation method. Spectra determination of intersystem crossing quantum yield and extinction coefficients of singlet-triplet transitions. Chem. Comm. 14: 446-447.

[33] Parker, C.A. 1968. Photoluminescence of solutions. Elsevier Publishing Company, Amsterdam-London-New York.

[34] Avakian, P., and E. Abramon. Singlet-Triplet Exciton Absorption Spectra in Naphthalene and Pyrene Crystals. J. Chem. Phys. 43 (3), 821-823, 1965.

[35] Gryczynski Z, Kimball J, Fudala R, Chavez J, Ceresa L, Szabelski M, Borejdo J, and Gryczynski I 2424 Photophysical properties of 2-Phenylindole in poly (vinyl alcohol) film at room temperature. Enhanced phosphorescence anisotropy with direct triplet state excitation Methods and Applications in Fluorescence. 8 014008

[36] Chavez J, Ceresa L, Kitchner E, Kimball J, Shtoyko T, Fudala R, Borejdo J, Gryczynski Z, and Gryczynski I 2424 On the possibility of direct triplet state excitation of indole Journal of Photochemistry and Photobiology B: Biology. 248 112297

[37] Chavez J, Ceresa L, Reeks J M, Strzhemechny Y M, Kimball J, Kitchner E, Gryczynski Z, and Gryczynski I 2426 Direct excitation of tryptophan phosphorescence. A new method for triplet states investigation Methods and Applications in Fluorescence. 10 029001

[38] Chavez J, Ceresa L, Kimball J, Kitchner E, Gryczynski Z and Gryczynski I 2426 Room temperature luminescence of 5-chloroindole Journal of Molecular Liquids. 400 123482

[39] Chavez J, Ceresa L, Kitchner E, Pham D, Gryczynski Z, and Gryczynski I 2427 Room temperature phosphorescence of 2-aminopyridine with direct triplet state excitation Spectrochimica Acta Part A: Molecular and Biomolecular Spectroscopy. 335 127040

[40] Chavez, J., L Ceresa, E Kitchner, D Pham, Z Gryczynsk, I. Gryczynski. 2023. Room Temperature Phosphorescence of 5, 6-Benzoquinoline. Methods and Applications in Fluorescence, Vol 11(2), p 025003.

[41] Alexander E, Chavez J, Ceresa L, Seung M, Pham D, Gryczynski Z, and Gryczynski I 2427 Room temperature phosphorescence of coumarin 106 with direct triplet state excitation Dyes and Pigments. 257 111433

[42] Su Y, Phua SZF, Li Y, Zhou X, Jana D, Liu G, Lim WQ, Ong WK, Yang C, Zhao Y, Ultralong room temperature phosphorescence for amorphous organic materials toward confidential information encryption and decryption. Sci. Adv. 2018. 4 (5), DOI: 10.1126/sciadv.aas9732.

[43] Lee D, Bolton O, Kim BC, Youk JH, Takayama S, Kim J, Room Temperature Phosphorescence of Metal-Free Organic Materials in Amorphous Polymer Matrices, J. Am. Chem. Soc. 2013. 135 (16), 6325–6329. DOI:10.1021/ja401769g

[44] Cai S, Ma H, Shi H, Wang H, Wang X, Xiao L, Ye W, Huang K, Cao X, Gan N, Ma C, Gu M, Song L, Xu H, Tao Y, Zhang C, Yao W, An Z, Huang W, Enabling long-lived organic room temperature phosphorescence in polymers by subunit interlocking. Nature Communications. 2019. 10, 4247. DOI: 10.1038/s41467-019-11749-x

[45] Gryczynski I, Kawski A, Nowaczyk K, Paszyc S, Skalski B, Temperature effect on the luminescence of synthesized Yt-based in PVA film, Biochem. Biophys. Res. Commun. 1981. 98 (4), 1070–1075. DOI: 10.1016/0006-291X(81)91220-1

[46] Gryczynski Z, Gryczynski I, Practical Fluorescence Spectroscopy. CRS Press, Taylor and Francis Group, 2020.

[47] Yang X., Yan D., Strongly Enhanced Long-Lived Persistent Room Temperature Phosphorescence Based on the Formation of Metal–Organic Hybrids. 2016. *Adv. Optical Mater*. **4**, 897-905.

[48] Gao R., Fang X., Yan D., Direct white-light emitting room-temperature-phosphorescence thin films with tunable two-color polarized emission through orientational hydrogen-bonding layer-by-layer assembly. 2018. *J. Mater. Chem. J. Mater. Chem. C,* **6**, 4444.

[49] Gao R., Fang X., Yan D., Recent developments in stimuli-responsive luminescent films. 2019. *J. Mater. Chem.* **7**, 3399-3412.

[50] Gao R., Kodaimati M.S., Yan D., Recent advances in persistent luminescence on molecular hybrid materials. 2021. *Chem. Soc. Rev.* **50**, 5564.

[51] Zhou B., Qi Z., Yan D., Highly Efficient and Direct Ultralong All-Phosphorescence from Metal-Organic Framework Photonic glases. 2022. *Angew. Chem. Int.Ed.,* **61**, e202208735..

[52] Higginbotham H. F., Okazaki M., de Silva P., Minakata S., Takeda Y., Data P., Heavy-Atom-Free Room-Temperature Phosphorescent Organic Light-Emitting Diodes Enabled by Excited States Engineering. 2021. *Appl. Mater. Interfaces*, **13**, 2899-2907.

[53] Liu S., Lin Y., Yan D., Hydrogen-bond organized 2D metal-organic microsheets: direct ultralong phosphorescence and color-tunable optical waveguides. 2022. *Science Bulletin,* **67,** 2076-2084.

[54] Gryczynski I, Kawski A, Nowaczyk K, Cherek H, Thermal deactivation of the lowest singlet and triplet excited states of acridine dyes in poly(vinyl alcohol) films, J. Photochem. 1985. 31 (2–3), 265–272. DOI:10.1016/0047-2670(85)85095-4

[55] Kawski A, Gryczynski I, Gryczynski Z, Fluorescence and phosphorescence anisotropy spectra of indole in poly (vinyl alcohol) film at room temperature. Z. Naturforsch. A. 1994. 49 (11), 1091. DOI: 10.1515/zna-1994-1118

[56] Kowalska-Baron A, Chan M, Gałecki K, Wysocki S, Photophysics of indole, tryptophan and N-acetyl-l-tryptophanamide (NATA): heavy atom effect. Spectrochim. Acta. A. Mol. Biomol. Spectrosc. 2012. 98, 282–289. DOI:10.1016/j.saa.2012.08.017

[57] Kowalska-Baron A, Gałecki K, Wysocki S, Room temperature phosphorescence study on the structural flexibility of single tryptophan containing proteins. Spectrochim. Acta. A. Mol. Biomol. Spectrosc. 2015. 134, 380–387. DOI: 10.1016/j.saa.2014.06.122

[58] Debye P, Edwards JO. Science. A note on the phosphorescence of proteins; 1952; 116:143. [PubMed: 14950214]

[59] Saviotti, M. and Galley, W. 1974. Room temperature phosphorescence and the dynamic aspects of protein structure. Proc. Natl. Acad. Sci. U.S.A. 71(10): 4154. -4158.

[60] Kai Y. and Imakubo K. 1979. Temperature dependence of the phosphorescence of heterogenous tryptophan residues in globular proteins between 293 and 77K. Photochem. Photobiol. 29:261-265.

[61] Domanus J, Strambini GB, Galley WC. 1980. Heterogeneity in the thermally-induced quenching of the phosphorescence of multi-tryptophan proteins. Photochem Photobiol. 1980;31(1):15-21.

[62] Strambini GB. 1983. Singular oxygen effects on the room-temperature phosphorescence of alcohol dehydrogenase from horse liver. Biophys. J. 43: 127-130.

[63] Strambini GB, E. Gabellieri. Intrinsic Phosphorescence from Proteins in the Solid State. Photochem. Photobiol. 1984. 39(6): 725- 729. 4. G.B. Strambini. ‘‘Tryptophan Phosphorescence as a Monitor of Protein Flexibility’’. J. Mol. Liq. 1989. 42: 155-165.

[64] Strambini G.B., and M. Gonnelli. 2010. Protein Phosphorescence Quenching: Distinction between Quencher Penetration and External Quenching Mechanisms. J.Phys.Chem.B, 114, 9691–9697

[65] Vanderkooi J., Calhoun D. and Englander, S. 1987. On the prevalence of room-temperature protein phosphorescence. Science. 236(4801):568-569.

[66] Papp, S, and Vanderkooi J. 1989. Tryptophan phosphorescence at room temperature as a tool to study protein structure and dynamics. Photochem. Photobiol. 49(6):775-84.

[67] Mersol, J., Steel, D. and Gafni, A.1993. Detection of intermediate protein conformations by room temperature tryptophan phosphorescence spectroscopy during the denaturation of Escherichia coli alkaline phosphatase. Biophys. Chem. 48:281-291.

[68] Fischer,C.J., Gafni, A, Steel D.G., and Schauerte, J.A. 2002. TheTriplet-State Lifetime of Indole in Aqueous and Viscous Environments: Significance to the Interpretation of Room Temperature Phosphorescence in Proteins. JACS,124, 10359-10366

[69] Draganski, A.R., M. G. Corradini, and R. D. Ludescher. 2015. Revisiting Time-Resolved Protein Phosphorescence. Applied Spectroscopy, Vol. 69, (9), Pages 1074-1081

[70] Valeur B. and Barberan-Santos MN, *Molecular Fluorescence: Principles and Applications* (Hoboken, New Jersey, United States of America: Wiley-VCH, 2012).

[71] Lakowicz, JR *Principles of Fluorescence Spectroscopy*, (Springer Science, New York, NY, 2006).

[72] Zhang Y., et al., Cross-Linked Polyphosphazene Nanospheres Boosting Long-Lived Organic Room-Temperature Phosphorescence. *J. Am. Chem. Soc.* 2022, 144, 13, 6107–6117

[73] Souza, B., Farias G., Neese F., and Izsak R., 2019. Predicting Phosphorescence Rates of Light Organic Molecules Using Time-Dependent Density Functional Theory and Path Integral Approach to Dynamics. J. Chem. Theory Comput. 15, 1896-1904.

[74] Zhao W., He Z., Tang B.Z., Nat. Rev. Mater. 2020, 5, 869-85

[75] Kenry, C. Chen, B. Liu, Nat. Commun. 2019, 10, 2111

[76] Gu L., Shi H., Bian L., Gu M., Ling K., Wang X., Ma H., Cai S., Ning W., Fu L., Nat. Photonics. 2019, 13, 406-11

[77] Su Y., Phua S.Z.F., Li Y., Zhou X., Jana D., Liu G., Lim W.Q., Ong W.K., Yang C., Zhao Y., Sci. Adv. 2018, 4, eaas9732

[78] Lü B., et al., Cell Rep. 2022, 3, 101015

[79] Ma H., Peng Q., An Z., Huang W., Shuai Z., J. Am. Chem. Soc. 2018, 141, 1010-5

[80] Gu L., Shi H., Miao C., Wu Q., Cheng Z., Cai S., Gu M., Ma C., Yao W., Gao Y., J. Mater. Chem. C. 2018, 6, 226-33

[81] Yao X., Ma H., Wang X., Wang H., Wang Q., Zou X., Song Z., Jia W., Li Y., Mao Y., Nat. Commun. 2022, 13, 4890

[82] Dann O., Bergen G., Demant G., Vol G., Trypanosomicidal diamidines of 2-phenylbenzofuran, 2-phenylindene, 2-phenylindole. 1971. *Justus Liebigs Ann. Chem*. **749**, 68-89.

[83] Russell W.C., Newman C., Williamson D.H. A simple cytochemical technique for demonstration of DNA in cells infected with mycoplasmas and viruses. 1975. *Nature* **253**, 461-462.

[84] Kapuscinski J., Skoczylas B. Fluorescent complexes of DNA with DAPI or DCI. 1978. *Nucleic Acids Res.* **5,** 3775-3799.

[85] Manzini G., Barcellona M.L., Avitabile M., Quadrifoglo F. Interaction of DAPI with natural and synthetic nucleic acids. 1983. *Nucleic Acids Res*. **11**, 8861-8876.

[86] Tanious F.A., Veal J.M., Buczak H., Ratmeyer L.S., Wilson W.D. DAPI binds differently to DNA and RNA: minor groove binding at AT sites and intercalation at AU sites. 1992. *Biochemistry* **31**, 3103-3112.

[87] Biancardi A., Biver T., Secco F., Mennucci B. An investigation of the photophysical properties of minor groove bound and intercalated DAPI through quantum-mechanical and spectroscopic tools. 2013. *Phys. Che. Chem. Phys* **15**, 4596-4603.

[88] Kapuscinski J., Szer W. Interactions of DAPI with synthetic polynucleotides. 1979. *Nucleic Acids Res*. **6,** 3519-3534.

[89] Ericsson S., Kim S.K., Kubista M., Norden B. Binding of DAPI to AT regions of DNA: evidence for an allosteric conformational change. 1993. *Biochemistry* 32, 2987-2998.

[90] Rocchi A., Di Castro M., Prantera G. Effect of DAPI on Chinese hamster chromosomes. 1980. *Cytogenet. Cell Gen*. **27**, 70-72.

[91] Schweizer D. Reverse fluorescent chromosome bainding with chromomycin and DAPI. 1976. *Chromosoma* **58**, 307-324.

[92] Barcellona M.L., Favilla R., van Berger J., Avitabile M., Ragusa N., Masotti L. DNA-DAPI intercallations: a comparative study employing fluorescence and UV spectroscopy. 1986. *Arch. Biochem. Biophys*. **22**, 11-16.

[93] Barcellona M.L., Gratton E. The fluorescence properties of a DNA probe DAPI. 1990. *Eur. Biophys. J.* **17**, 315-323.

[84] Szabo A.G., Krajcarski D.T., Cavatorta P., Masotti L., Barcellona M.L. Excited state pKa behaviour of DAPI-nucleic acid complexes. 1986. *Photochem. Phootobiol*. **44,** 143-150.

[95] Lakowicz, J.R. and Gryczynski, I. Fluorescence Intensity and Anisotropy Decay of the 4',6-Diamidino-2-phenylindole-DNA Complex Resulting from One-Photon and Two-Photon Excitation. 1992. *J. Fluoresc*. **2**,117-122.

[96] Kubista M., Akerman B., Albinsson B. Characterization of the Electronic Structure of 4'-6-diamidino-2-phenylindole. 1989. *J. Am. Chem. Soc.*, **111**, 7031-7035.

[97] Karg T.J., Golic K.G. Photoconversion of DAPI and Hoechst dyes to green and red emitting forms after exposure to UV excitation. 2018. *Chromosoma* **127 (2),** 235-245.

[98] Misra A., Ozarowski A., Maki A.H. Phosphorescence and Optically Detected Magnetic Resonance of 4'-6-diamidino-2-phenylindole (DAPI) and its Complexes with $[d(CGACGTCG)]_2$ and $[d(GGCCAATTGG)]_2$. 2002. *Biochemistry* **41,** 6477-6482.

[99] Reynolds G.A. and Drexhage K.H., New coumarin dyes with rigidized structure for flashlamp-pumped. 1975. *Optics Comm*. **13 (3)**, 222-225.

[100] Honda T, Fujii I, Hirayama N, Aoyama N, Miike A, Organic Compounds: Coumarin 106, C18H19NO2 Acta Cryst. 1996, C52, 364-365. DOI: 10.1107/S0108270195010845

[101] Cao D, Liu Z, Verwilst P, Koo S, Jangjili P, Kim JS, Lin W, Coumarin-Based Small-Molecule Fluorescent Chemosensors. Chem. Rev. 2019 119 (18), 10403-10519. DOI: 10.1021/acs.chemrev.9b00145

[102] Fallarero A, Oinonen P, Gupta S, Blom P, Galkin A, Mohan CG, Vuorela PM, Inhibition of acetylcholinesterase by coumarins: the case of coumarin 106. Pharmacological Research 2008, 58, 215-221.

[103] Sun X, Liu T, Sun G, Wang X, Synthesis and application of coumarin fluorescence probes (Review Article) RSC Adv., 2020, 10, 10826-10847.

[104] Li LD, Yang SZ, Room temperature phosphorescence properties of 27 coumarin derivatives on filter paper Anal. Chimica Acta 1994, 296, 99-105.

[105] Wu, Hao (August 2020). "An overview of tailoring strain delocalization for strength-ductility synergy". *Progress in Materials Science*. **113**: 100675.

[106] Verhoeven, J.D. *Fundamentals of Physical Metallurgy*, Wiley, New York, 1975, p. 326

[107] Humphreys, F. J.; Prangnell, P. B.; Bowen, J. R.; Gholinia, A.; Harris, C.; Hutchinson, B.; Brown, L. M.; Stowell, M. J.; Sevillano, J. Gil; Withers, P. J. (1999). *Philosophical Transactions: Mathematical, Physical and Engineering Sciences.* **357** (1756): 1663–1681.

[108] Fukumori T., Nakaoki T., Significant Improvement of Mechanical Properties for Polyvinyl Alcohol Film Prepared from Freeze/Thaw Cycled Gel. 2013. *Open J. Polym. Mater.* **3** 38808.

[109] Deb S., Sarkar D. Effect of annealing temperature on optical properties of silver-PVA nanocomposite. 2018. *Optik* **157** 1115–1121.

[110] Wang, S., Komvopoulos, K. 2020. Structure evolution during deposition and thermal annealing of amorphous carbon ultrathin films investigated by molecular dynamics simulations. *Sci Rep* **10**, 8089

[111] Wei X., Yang J., Hu L., Cao Y., Lai J., Cao F., Gu J. and Cao X. 2021. Recent advances in room temperature phosphorescent carbon dots: preparation, mechanism, and applications. *J. Mater. Chem. C*. **9,** 4425.

[112] Bao X., Ushakova E.V., Liu E., Zhou Z., Li D., Zhou D., Qu S., and Rogach A.L., 2019. On–Off switching of the phosphorescence signal in a carbon dot/polyvinyl alcohol composite for multiple data encryption. *Nanoscale*. 30

[113] Zheng C., Tao S., Yang B. 2023. Polymer-Structure-Induced Room Temperature Phosphorescence of Carbon Dot Materials. *Small Struct.* **4.** 2200327.

[114] Tian Z., Li D., 2018. Multilevel Data Encryption Using Thermal-Treatment Controlled Room Temperature Phosphorescence Of Carbon Dot/PolyVinylAlcohol Composites. *Adv. Sci.* **1800795**.

[115] Thomas H., Haase K., Achenbach T., Bärschneider T., Kirch A., Talnack F., Mannsfeld S.C.B., and Reineke S., 2022. *Front. Phys.* **10** 841413

[116] Thomas D., Cebe P. Self-nucleation and crystallization of polyvinyl alcohol. 2017. J. Therm. Anal. And Calorimetry **127**, 885-894.

[117] Wong K.K., Zinke-Almang M., Wan W. Effect of annealing on aqueous stability and elastic modulus of electro-spun poly(vinyl alcohol) fibers. 2010. J. Mater. Sci. 45, 2456-2465.

[118] Alexander E., Ceresa L., Pham D., Gryczynski Z., Gryczynski I., Effect of Annealing on the room temperature luminescence of coumarin 106 in PVA Films. 2024. *Methods Appl. Fluoresc.* **12**, 015005.

[119] Alexander E., Lee B., Pham D., Garcia-Rodriguez S., Gryczynski Z., and Gryczynski I., Photophysical Properties of DAPI in PVA Films. Possibiliti of Room Temperature Phosphorescence.2024. *Anal. Biochem.* 689, 115498.

[120] Strzhemechny, Y. (2024) *Chapter 10: Angular Momentum.* Quantum Mechanics Class notes. Published.

[121] Strzhemechny, Y. (2024) *Chapter 4: Two Level Systems.* Quantum Mechanics Class notes. Published.

[122] Strzhemechny, Y. (2024) *Chapter 9: Spin.* Quantum Mechanics Class notes. Published.

[123] Strzhemechny, Y. (2024) *Chapter 14: Systems of Identical Particles* Quantum Mechanics Class notes. Published.

[124] Harris DC., Bertolucci MD., Symmetry and Spectroscopy: An introduction to vibrational and electronic spectroscopy, (Dover Publications, Garden City, NY, 1978)

[125] Spin-Orbit Coupling. (2023, May 3). https://chem.libretexts.org/@go/page/352416

[126] Strzhemechny, Y. (2024) *Chapter 11, 12: Stationary Perturbation Theory and Its Applications.* Quantum Mechanics Class notes. Published.

[127] Wong K.K., Zinke-Almang M., Wan W. Effect of annealing on aqueous stability and elastic modulus of electro-spun poly(vinyl alcohol) fibers. 2010. J. Mater. Sci. 45, 2456-2465.

[128] J. Kimball, Ph.D. Thesis, Texas Christian University, 2015, (online TCU Library)

[129] E. Kitchner, MS. Thesis, Texas Christian University, 2021 (online TCU Library)

[130] L. Ceresa, M.S. Thesis, Texas Christian University, 2020, (online TCU Library)

[131] Sillen A, Engelborghs Y. 1998. The correct use of 'average' fluorescence parameters Photochem. Photobiol;67:475–86.

[132] Jameson D, *Introduction to Fluorescence* (CRC Press, Taylor & Francis Group, Boca Raton, Florida, 2014)

[133] Jablonski A. 1960. On the notion of emission anisotropy. Bull l'Acad Pol Sci, Ser A 8:259-264

[134] Weber G, 1966. Polariztion of the fluorescence of solutions. In Fluorescence and phosophorescence analysis, pp. 217-240. Ed DM Hercules. John Wiley & Sons, New York

[135] Perrin F, Ann. Phys. 1929. 10, 12, 169-275.

[136] Perrin F, Acta. Phys. Pot. 5, 335 (1936).

[137] Steiner R.F 1991. Fluorescence Anisotropy: Theory and applications, in Lakowicz J.R. Topics in Fluorescence Spectroscopy, Vol. 2, Principles, Plenum Press, New York, pp 127-176

[138] Jablonski A. 19 70. Anisotropy of Fluorescence molecules excited by excitation transfer. Acta Phys Pol A 38: 453-458

[139] Srithep, Y (2012). "IEffects of Annealing Time and Temperature on the Crystallinity and Heat Resistance Behavior of Injection-Molded Poly(lactic acid)" Polymer Engineering and Science. **53** (3).

[140] Tsioptsias, C., Fardis, D., Ntampou, X., Tsivintzelis, I., and Panayiotou, C. 2023. Thermal Behavior of Poly(vinyl alcohol) in the Form of Physcially Crosslinked Film. *Polymers* **15** 1843.

[141] Samsuri A. B, Abdullahi A. A, Degration of Natural Rubber and Syntehtic Elastomers. Reference Module in *Mat. Sci and Mat Eng.* 2017.

[142] Karg T.J., Golic K.G. Photoconversion of DAPI and Hoechst dyes to green and red emitting forms after exposure to UV excitation. 2018. Chromosoma 127 (2), 235-245.

[143] Eaton DF, Reference materials for fluorescence measurement. Pure Appl. Chem. 1998. 60, 1107-1114. DOI: 10.1351/pac198860071107

[144] Kimball J, Chavez J, Ceresa L, Kitchner E, Nurekeyev Z, Doan H, Szabelski M, Borejdo J, Gryczynski I, and Gryczynski Z. 2020. On the origin and correction for inner filter effects in fluorescence Part I: primary inner filter effect-the proper approach for sample absorbance correction. *Methods Appl. Fluoresc.* **8** 033002.

[145] Ceresa L, Kimball J, Chavez J, Kitchner E, Nurekeyev Z, Doan H, Borejdo J, Gryczynski I, and Gryczynski Z. 2021. On the Origin and Correction for Inner Filter Effects in Fluorescence. Part II: Secondary Inner Filter Effect -The Proper Use of Front-Face Configuration for Highly Absorbing and Scattering Samples. *Methods Appl. Fluorescence.* **9** 035005.

Note: Passages in this thesis have been quoted verbatim from the following sources:

- **Emma Alexander,** Bong Lee, Danh Pham, Samuel Garcia- Rodriguez, Zygmunt Gryczynski, and Ignacy Gryczynski. *Photophysical Properties of DAPI in PVA Films. Possibility of Room Temperature Phosphorescence.* Anal. Biochem. (February 2024).
- **Emma Alexander,** Luca Ceresa, Danh Pham, Zygmunt Gryczynski, Ignacy Gryczynski. *Effect of Annealing on the Room Temperature Luminescence of Coumarin 106 in PVA Films.* Methods Appl. Fluoresc. **12** (2024) 015005.
- **Emma Alexander**, Jose Chavez, Luca Ceresa, Michael Seung, Danh Pham, Zygmunt Gryczynski, Ignacy Gryczynski. *Room temperature phosphorescence of coumarin 106 with direct triplet state excitation.* Dyes Pigm. **217** (2023) 111389

VITA

Emma Alexander was born July 6, 1997, in Poughkeepsie, New York. She is the daughter of Peter and Kimberly Kitchner. A 2015 graduate of Hudson Falls High School, Hudson Fall, New York, she received a Bachelor of Science degree with majors in Physics and Mathematics from St. Lawrence University, Canton, New York, in 2019.

Emma then went to Texas Christian University, earning her Master of Science in 2021. She continued to pursue her degree and obtained her PhD in 2024. While working on her Doctorate in Biophysics, she held a Teaching Assistantship position from 2019 to 2024. She also held the Green Fellowship in 2019-2020.

She is married to Dalton Alexander.

VITA

Personal — Emma Alexander

Background
Poughkeepsie, New York
Daughter of Peter and Kimberly Kitchner
Married Dalton Alexander, April 8, 2023

Education

PhD in Biophysics — 2024
Texas Christian University
Fort Worth, Texas

Masters of Science, Physics, — 2021
Texas Christian University
Fort Worth, Texas

Bachelors of Science, Physics and Mathematics — 2019
St. Lawrence University
Canton, New York

Advanced Regents Diploma — 2015
Hudson Falls High School
Hudson Falls, New York

Experiences

Teaching Assistantship, Texas Christian University — 2019-2024
Fort Worth, Texas

Research Assistantship, Texas Christian University — 2019-2024
Luminescence Lab
Advisor: Dr. Zygmunt Gryczynski
Fort Worth Texas

Teaching Assistantship, St. Lawrence University — 2017-2019
Canton, New York

NSF REU Summer Research, SUNY Geneseo — 2018
Quantum Optics
Advisor: Dr. George Marcus

Publications (* first author paper)

1. ***Emma Alexander,** Bong Lee, Danh Pham, Samuel Garcia- Rodriguez, Zygmunt Gryczynski, and Ignacy Gryczynski. *Photophysical Properties of DAPI in PVA Films. Possibility of Room Temperature Phosphorescence.* Anal. Biochem. (February 2024).
2. ***Emma Alexander,** Luca Ceresa, Danh Pham, Zygmunt Gryczynski, Ignacy Gryczynski. *Effect of Annealing on the Room Temperature Luminescence of Coumarin 106 in PVA Films.* Methods Appl. Fluoresc. (November 2023).
3. ***Emma Alexander**, Jose Chavez, Luca Ceresa, Michael Seung, Danh Pham, Zygmunt Gryczynski, Ignacy Gryczynski. *Room temperature phosphorescence of coumarin 106 with direct triplet state excitation.* Dyes Pigm. (May 2023)
4. Luca Ceresa, Jose Chavez, Magdalena Bus, Bruce Budowle, **Emma Kitchner**, Joseph Kimball, Zygmunt Gryczynski, Ignacy Gryczynski, *Multi Intercalators FRET Enhanced Detection of Minute Amounts of DNA.* Eur. Biophys. J. (May 2023)
5. Jose Chavez*, Luca Ceresa, **Emma Kitchner**, Danh Pham, Zygmunt Gryczynski, and Ignacy Gryczynski. *Room Temperature Phosphorescence of 5,6- Benzoquinoline.* Methods Appl. Fluoresc. (April 2023)
6. Jose Chavez*, Luca Ceresa, **Emma Kitchner**, Danh Pham, Zygmunt Gryczynski, and Ignacy Gryczynski. *Room temperature phosphorescence of 2-aminopyridine with direct triple state excitation*. Spectrochim. Acta A Mol. Biomol. Spectrosc. (March 2023)
7. ***Emma Kitchner,** Michael Seung, Jose Chavez, Luca Ceresa, Joseph Kimball, Ignacy Gryczynski, and Zygmunt Gryczynski. *Fluorescence Measurements: Importance of G-Factor Correction, Magic Angle and Observation Wavelengths.* Methods Appl. Fluoresc. (Sept 2022)
8. Luca Ceresa, Jose Chavez, **Emma Kitchner,** Joseph Kimball, Ignacy Gryczynski, Zygmunt Gryczynski. *Imaging and Detection of Long-Lived Fluorescence Probes in Presence of Highly Emissive Scattering Background.* Exp. Biol. Med. (August 2022)
9. Jose Chavez, Luca Ceresa, Joseph Kimball, **Emma Kitchner**, Zygmunt Gryczynski, Ignacy Gryczynski**.** *Room Temperature Luminescence of 5-Chloroindole.* J. Mol. Liq. (August 2022)
10. Luca Ceresa, Jose Chavez, **Emma Kitchner**, Magdalena Bus, Bruce Budowle, Joseph Kimball, Zygmunt Gryczynski, Ignacy Gryczynski. *FRET Enhanced Detection of Minute Amounts of DNA.* Anal. Chem (March 2022)
11. J. Chavez, Luca Ceresa, John M. Reeks, Yuri M. Strzhemechny, Joseph Kimball, **Emma Kitchner**, Zygmunt Gryczynski, and Ignacy Gryczynski. *Direct Excitation of Tryptophan Phosphorescence. A New Method for Triplet States Investigation.* Methods Appl. Fluoresc. (Jan. 2022)
12. Luca Ceresa, **Emma Kitchner**, Michael Seung, Magdalena M. Bus, Bruce Budowle, Jose Chavez, Ignacy Gryczynski, and Zygmunt Gryczynski. *A Novel Approach to Imaging and Visualization of Minute Amounts of DNA in Small Volume Samples.* Analyst (Sept. 2021)
13. Luca Ceresa Joseph Kimball, Jose Chavez, **Emma Kitchner,** Zhangatay Nurekeyev, Hung Doan, Julian Borejdo, Ignacy Gryczynski, and Zygmunt Gryczynski. *On the Origin and Correction for Inner Filter Effects in Fluorescence. Part II: Secondary Inner Filter Effect -The Proper Use of Front-Face Configuration for Highly Absorbing and Scattering Sample*. Methods Appl. Fluoresc. (May 2021)

14. ***Emma Kitchner,** Jose Chavez, Luca Ceresa, Magdalena M. Bus, Bruce Budowle, and Zygmunt Gryczynski. *A novel approach for visualization and localization of small amounts of DNA on swabs to improve DNA collection and recovery process.* Analyst (Jan. 2021)
15. Jose Chavez Joseph Kimball, Luca Ceresa, **Emma Kitchner,** Tanya Shtoyko, Rafal Fudala, Julian Borejdo, Zygmunt Gryczynski, and Ignacy Gryczynski. *Luminescence Properties of 5-Bromoindole in PVA Films at Room Temperature. Direct Triplet State Excitation.* J. Lumin. (November 2020)
16. Joe Kimball, Jose Chavez, Luca Ceresa, **Emma Kitchner**, Zhangatay Nurekeyev, Hung Doan, Mariusz Szabelski, Julian Borejdo, Ignacy Gryczynski, Zygmunt Gryczynski. *On the Origin and Correction for Inner Filter Effects in Fluorescence. Part I: Primary Inner Filter Effect -The Proper Approach for Sample Absorbance Correction.* Methods Appl. Fluoresc. (May 2020)
17. Jose Chavez, Luca Ceresa, **Emma Kitchner**, Joseph Kimball, Tanya Shtoyko, Rafal Fudala, Julian Borejdo, Zygmunt Gryczynski, Ignacy Gryczynski. *On the Possibility of Direct Triplet State Excitation of Indole.* J. Photochem. Photobiol. B. Biol. (May 2020)

Abstract

ROOM TEMPERATURE PHOSPHORESCENCE: INVESTIGATION INTO EXTERNAL PERTURBATION OF PVA FILM TO ENHANCE SPIN-ORBIT COUPLING

By Emma Alexander, 2024

Department of Physics and Astronomy

Texas Christian University

Thesis advisor: Dr. Zygmunt "Karol" Gryczynski

In this thesis, we present the Room Temperature Phosphorescence (RTP) of 4'-6-diamidino-2-phenylindole (DAPI) and Coumarin 106 (C106) embedded in PVA poly ((vinyl)alcohol) film, respectively.

Our previous studies concluded that chromophores are perturbed significantly enough to exhibit efficient phosphorescence emission when embedded into the PVA film. Furthermore, we observed that for some compounds embedded into the PVA film, we can observe direct triplet state excitation followed by strong phosphorescence emission. We also noticed that phosphorescence efficiency depends on PVA film preparation. So, we want to investigate modifications in PVA preparation/treatment and how the modifications may enhance Spin-Orbit Coupling (SOC). Our long-term project goal is to investigate if external conditions (conditions we can control/change externally, like electromagnetic fields) can affect SOC and lead to RTP emission in liquid solutions.

We found that an efficient room temperature phosphorescence (RTP) of DAPI has been observed with UV and blue light excitations. For C106, we also found an efficient RTP. We observed C106 directly excited phosphorescence at 465 nm, well outside the absorption band.

Then, we used C106 samples to study the effects of external modifications to the PVA treatments.

We found that the PVA polymer films change their optical properties after annealing at higher temperatures. Whereas the fluorescence intensity of C106 in PVA films modestly decreases with annealing, the phosphorescence depends dramatically and progressively increases by many folds. We believe this increase in the phosphorescence intensities results from increased intersystem crossing (ISC), which also decreases fluorescence. The phosphorescence lifetime decreases with annealing while the phosphorescence intensity increases.

We could not confirm the validity of investigating any external conditions that can affect SOC. However, we feel confident in our initial findings with annealing to say that it is possible to manipulate the PVA film preparation/treatment to enhance SOC.